Lightness of a Higgs boson and spontaneous *CP*-violation in the Lee model: An alternative scenario

Ying-nan Mao[1,4,*] and Shou-hua Zhu[1,2,3,†]

[1]*Institute of Theoretical Physics & State Key Laboratory of Nuclear Physics and Technology, Peking University, Beijing 100871, China*

[2]*Collaborative Innovation Center of Quantum Matter, Beijing 100871, China*

[3]*Center for High Energy Physics, Peking University, Beijing 100871, China*

[4]*Center for Future High Energy Physics & Theoretical Physics Division, Institute of High Energy Physics, Chinese Academy of Sciences, Beijing 100049, China*

(Received 6 February 2016; revised manuscript received 18 July 2016; published 9 September 2016; publisher error corrected 19 September 2016)

Based on the weakly coupled spontaneous *CP*-violation two-Higgs-doublet model (called the Lee model) and the mechanism to generate the correlation between the smallness of *CP* violation and the lightness of the scalar mass, as we proposed earlier, we predict a light *CP* mixing scalar η in which the pseudoscalar component is dominant. It is a natural scenario in which $m_\eta \sim \mathcal{O}(10\ \mathrm{GeV}) \ll v$. It means new physics might be hidden below the electroweak scale v. Masses of all other scalars (h, H, $H^\pm$) should be around the electroweak scale v. Among them, the 125 GeV Higgs boson (h) couplings are standard-model-like, and the charged Higgs boson ($H^\pm$) mass should be around the heaviest neutral scalar (H) mass. We discussed all experimental constraints and showed that this scenario is still allowed by data. The strictest constraints come from the flavor violation experiments and the electric dipole moments of the electron and neutron. We also discussed the future tests for this scenario. It is possible to discover the extra scalars or exclude this scenario at future colliders, especially at the LHC and e^+e^- colliders with $\mathcal{O}(\mathrm{ab}^{-1})$ luminosity. We also pointed out that the Z-mediated Higgs pair production via $e^+e^- \to h_i h_j$ (h_i, h_j stand for two of the η, h, H) would be the key observable to confirm or exclude *CP* violation in the Higgs sector. The sensitivity to test this scenario is worth studying in greater detail.

DOI: 10.1103/PhysRevD.94.055008

I. INTRODUCTION

The realization of electroweak symmetry breaking and *CP* violation are two important topics both in the standard model (SM) and beyond the standard model (BSM). It is also attractive to relate them with each other. In our previous work [1], we proposed the correlation between the lightness of the Higgs boson and the smallness of *CP* violation. In this paper, we will continue to explore an alternative natural scenario and its phenomenology.

In 1964, the Higgs mechanism [2] was proposed. In the Higgs mechanism, a scalar doublet with nontrivial vacuum expectation value (VEV) was introduced to break the electroweak gauge symmetry spontaneously. After spontaneous gauge symmetry breaking in the SM, there exists a scalar named the Higgs boson.[1] In July 2012, both ATLAS [4] and CMS [5] collaborations at the LHC discovered a new boson with its mass around 125 GeV [6]. The subsequent measurements by CMS and ATLAS [7–9] on its signal strengths showed that the scalar behaves similarly to the SM Higgs boson. However, there is still plenty of room for the BSM. In some BSM models, there exist new light particles which may appear in the final states during Higgs decay processes. For example, in the next-to-minimal super-symmetric standard model (NMSSM) [10], the simplest little Higgs model (SLH) [11–13], or the left-right-twin-Higgs model (LRTH) [14,15], a light scalar η with its mass of $\mathcal{O}(10)$ GeV will naturally appear. For some cases in 2HDM [16–20], a light scalar η is allowed as well, though there are strict constraints on them. If $m_\eta < m_h/2 = 62.5$ GeV, there would be an exotic decay channel $h \to \eta\eta$, while if $m_\eta < m_h - m_Z = 34$ GeV, an exotic decay channel $h \to Z\eta$ should also be open. There is no evidence for exotic Higgs decay channels at the LHC until now, and the constraints on the exotic Higgs decay branching ratio are set to be $\mathrm{Br}_{\mathrm{exo}} \lesssim (20\text{–}30)\%$ [21] if the production rate of the Higgs boson is close to that in the SM. The spin-parity property for the Higgs boson is expected to be 0^+ in the SM. Experimentally, a pure pseudoscalar state (0^-) is excluded at over 3σ [22–24], but a mixing state is still allowed; thus, the spacious room for BSM scenarios has not been closed yet.

Theoretically, *CP* violation in SM is induced by the Kobayashi and Maskawa (K-M) mechanism [25] proposed

*maoyingnan@pku.edu.cn, maoyn@ihep.ac.cn

†shzhu@pku.edu.cn

[1]There may exist more particles in the extension of SM. For example, in the two-Higgs-doublet model (2HDM) [3] in which two scalar doublets were introduced, there exist five scalars. Two of them are charged and three of them are neutral.

by Kobayashi and Maskawa in 1973. They proved that a nontrivial phase which leads to CP violation in quark mixing matrix (called the CKM matrix [25,26]) would appear if there exist three or more generations of quarks. The CKM matrix is usually parametrized as the Wolfenstein formalism [27]

$$V_{\mathrm{CKM}} = \begin{pmatrix} 1-\lambda^2/2 & \lambda & A\lambda^3(\rho-i\eta) \\ -\lambda & 1-\lambda^2/2 & A\lambda^2 \\ A\lambda^3(1-\rho-i\eta) & -A\lambda^2 & 1 \end{pmatrix} + \mathcal{O}(\lambda^4). \quad (1)$$

The Jarlskog invariant J [28] defined as

$$\det\left(\mathrm{i}[M_U M_U^\dagger, M_D M_D^\dagger]\right) = 2J\prod_{i<j}(m_{U_i}^2 - m_{U_j}^2)\prod_{i<j}(m_{D_i}^2 - m_{D_j}^2) \quad (2)$$

measures the effects of CP violation where $M_{U(D)}$ is the mass matrix for up- (down-) type quarks. $J \approx \lambda^6 A^2 \eta \approx 3 \times 10^{-5}$ [29] means CP violation in the SM is small. Experimentally, in the K- and B-meson systems, several kinds of CP violation have been discovered [29] which represent the success of the K-M mechanism. However, it is still attractive to search for new sources of CP violation, not only to search for BSM physics but also to understand the matter-antimatter asymmetry in the Universe [29,30]. SM itself cannot provide enough baryogenesis effects [29–32], but in some extensions of SM, for example, 2HDM with CP violation in the Higgs sector, it is possible to generate large enough baryogenesis effect [31,33].

The Lee model [34] is a possible way to connect the Higgs mechanism and CP violation with each other. It was proposed by Lee in 1973 as the first 2HDM. In the Lee model, the Lagrangian is required to be CP conserved, but the VEV of one Higgs doublet can be complex; thus, the CP symmetry is spontaneously broken due to the complex vacuum. In this case, the neutral scalars are CP mixing states so that CP violation effects should occur in the Higgs sector. All the three neutral scalars should couple to massive gauge bosons with the effective interaction,

$$\mathcal{L}_{h_i VV} = \sum_i c_{i,V} h_i \left(\frac{2m_W^2}{v} W^{+\mu} W_\mu^- + \frac{m_Z^2}{v} Z^\mu Z_\mu\right), \quad (3)$$

where $c_{i,V} \equiv g_{h_i VV}/g_{hVV,\mathrm{SM}}$ is the ratio between the $h_i VV$ coupling strength and that in SM. $c_{1,V}^2 + c_{2,V}^2 + c_{3,V}^2 = 1$ due to the mechanism of spontaneous gauge symmetry breaking. The quantity

$$K \equiv c_{1,V} c_{2,V} c_{3,V} \quad (4)$$

measures the CP-violation effects in the Higgs sector [3,35] when the masses of the neutral scalars are nondegenerate.[2] In our recent paper [1], we proposed the correlation between the lightness of the Higgs boson and the smallness of CP violation through small $t_\beta s_\xi$ in the Lee model.[3] In that paper, we treated the 125 GeV scalar as the lightest one; thus, it implied a strongly interacted scenario beyond [36]. However, another natural scenario with a weakly interacted scalar in which the heavy scalars have the mass $m_i \sim \mathcal{O}(v)$ is also possible where $v = 246$ GeV is the VEV of the scalar doublet in SM. In this scenario, the Lee model would predict a light scalar η with mass $m_\eta \ll v$ for the small $t_\beta s_\xi$ case based on our paper [1]. In this paper, we will discuss this scenario and its phenomenology.

This paper is organized as follows. In Sec. II, we introduce the Lee model and its main properties. In Sec. III, we discuss the constraints for this scenario by recent experiments, including data from both high- and low-energy phenomena. In Sec. IV, we consider the predictions and future tests for this scenario. Section V contains our conclusions and discussions.

II. THE LEE MODEL AND A LIGHT SCALAR

In the Lee model [34], the Lagrangian is required to be CP conserved in both scalar and Yukawa sectors. For the scalar sector,

$$\mathcal{L} = (D_\mu \phi_1)^\dagger (D^\mu \phi_1) + (D_\mu \phi_2)^\dagger (D^\mu \phi_2) - V(\phi_1, \phi_2) \quad (5)$$

in which the scalar potential

$$V(\phi_1,\phi_2) = \mu_1^2 R_{11} + \mu_2^2 R_{22} + \lambda_1 R_{11}^2 + \lambda_2 R_{11} R_{12} + \lambda_3 R_{11} R_{22} + \lambda_4 R_{12}^2 + \lambda_5 R_{12} R_{22} + \lambda_6 R_{22}^2 + \lambda_7 I_{12}^2. \quad (6)$$

Here the scalar doublets

$$\phi_1 = \begin{pmatrix} \phi_1^+ \\ \frac{v_1 + R_1 + iI_1}{\sqrt{2}} \end{pmatrix}, \qquad \phi_2 = \begin{pmatrix} \phi_2^+ \\ \frac{v_2 e^{i\xi} + R_2 + iI_2}{\sqrt{2}} \end{pmatrix} \quad (7)$$

and $R(I)_{ij}$ denotes the real (imaginary) part of $\phi_i^\dagger \phi_j$.[4] $\sqrt{v_1^2 + v_2^2} = v = 246$ GeV. The general Yukawa couplings can be written as

[2] If at least two of the scalars have the same mass, we can always perform a field rotation between them to keep at least one $c_{i,V} = 0$; thus, there would be no CP violation in the Higgs sector.

[3] The parameters will be defined in the next section or see [1].

[4] We can always perform a rotation between ϕ_1 and ϕ_2 to keep the term proportional to R_{12} vanish.

$$\mathcal{L}_y = -\bar{Q}_{Li}((Y_{1d})_{ij}\phi_1 + (Y_{2d})_{ij}\phi_2)D_{Rj} - \bar{Q}_{Li}((Y_{1u})_{ij}\tilde{\phi}_1 + (Y_{2u})_{ij}\tilde{\phi}_2)U_{Rj}, \quad (8)$$

where all coupling constants should be real and $\tilde{\phi}_i \equiv i\sigma_2\phi_i^*$. We choose the type III [3,37] Yukawa couplings because there is no additional discrete symmetry to forbid any term in (8). It is possible to generate correct fermion mass spectrum and CKM matrix from (8), for example, see [38,39].

We should minimize the potential (6). For some parameter choices, there is a nonzero ξ which means the spontaneous CP violation.[5] If v_1, v_2, $\xi \neq 0$, we have

$$\mu_1^2 = -\lambda_1 v_1^2 - \frac{\lambda_3+\lambda_7}{2}v_2^2 - \frac{\lambda_2}{2}v_1 v_2 \cos\xi; \quad (9)$$

$$\mu_2^2 = -\frac{\lambda_3+\lambda_7}{2}v_1^2 - \lambda_6 v_2^2 - \frac{\lambda_5}{2}v_1 v_2 \cos\xi; \quad (10)$$

$$0 = \frac{\lambda_2}{2}v_1^2 + \frac{\lambda_5}{2}v_2^2 + (\lambda_4-\lambda_7)v_1 v_2 \cos\xi. \quad (11)$$

$|\lambda_2 v_1^2 + \lambda_5 v_2^2| < 2|\lambda_4-\lambda_7|v_1 v_2$ is required to keep $\xi \neq 0$. Define $s_\alpha \equiv \sin\alpha$, $c_\alpha \equiv \cos\alpha$, $t_\alpha \equiv \tan\alpha$ in the following parts of this paper, and $t_\beta \equiv v_2/v_1$ is the ratio of the VEVs for scalar doublets. The vacuum stability conditions can be found in [3] or Appendix. A in [1]. The Goldstone fields can be written as

$$G^\pm = c_\beta\phi_1^\pm + e^{\mp i\xi}s_\beta\phi_2^\pm; \quad (12)$$

$$G^0 = c_\beta I_1 + s_\beta c_\xi I_2 - s_\beta s_\xi R_2. \quad (13)$$

The charged Higgs field is orthogonal to the corresponding charged Goldstone field as

$$H^\pm = -e^{\pm i\xi}s_\beta\phi_1^\pm + c_\beta\phi_2^\pm \quad (14)$$

with the mass square

$$m_\pm^2 = -\frac{\lambda_7}{2}v^2. \quad (15)$$

The symmetric mass matrix $\tilde{m}$ for neutral scalars is written as [1]

$$\begin{pmatrix} (\lambda_4-\lambda_7)s_\xi^2 & -((\lambda_4-\lambda_7)s_\beta c_\xi + \lambda_2 c_\beta)s_\xi & -((\lambda_4-\lambda_7)c_\beta c_\xi + \lambda_5 s_\beta)s_\xi \\ & 4\lambda_1 c_\beta^2 + \lambda_2 s_{2\beta}c_\xi + (\lambda_4-\lambda_7)s_\beta^2 c_\xi^2 & ((\lambda_3+\lambda_7) + (\lambda_4-\lambda_7)c_\xi^2/2)s_{2\beta} \\ & & +\lambda_2 c_\beta^2 c_\xi + \lambda_5 s_\beta^2 c_\xi \\ & & (\lambda_4-\lambda_7)c_\beta^2 c_\xi^2 \\ & & +\lambda_5 s_{2\beta}c_\xi + 4\lambda_6 s_\beta^2 \end{pmatrix} \quad (16)$$

in the basis $(-s_\beta I_1 + c_\beta c_\xi I_2 - c_\beta s_\xi R_2, R_1, s_\xi I_2 + c_\xi R_2)^T$ in unit of $v^2/2$. To solve the eigenvalue equation with perturbation method,[6] we should expand $\tilde{m}$ in powers of $(t_\beta s_\xi)$ in small t_β limit as

$$\tilde{m} = \tilde{m}_0 + (t_\beta s_\xi)\tilde{m}_1 + (t_\beta s_\xi)^2\tilde{m}_2 + \ldots. \quad (17)$$

For the two heavy scalars, we have [1]

$$m_{h,H}^2 = \frac{v^2}{2}((\tilde{m}_0)_{22(33)} + \mathcal{O}(t_\beta s_\xi)), \quad (18)$$

where

$$(\tilde{m}_0)_{22(33)} = \frac{4\lambda_1+\lambda_4-\lambda_7}{2} \mp \left(\frac{4\lambda_1-(\lambda_4-\lambda_7)}{2}c_{2\theta} + \lambda_2 s_{2\theta}\right). \quad (19)$$

Here $\theta = (1/2)\arctan(2\lambda_2/(4\lambda_1-\lambda_4+\lambda_7))$ labels the mixing angle of the real parts of the two scalar doublets. The scalar fields

$$\begin{pmatrix} h \\ H \end{pmatrix} = \begin{pmatrix} c_\theta & s_\theta \\ -s_\theta & c_\theta \end{pmatrix}\begin{pmatrix} R_1 \\ R_2 \end{pmatrix} + \mathcal{O}(t_\beta s_\xi). \quad (20)$$

We treat the lighter one as $m_h = \sqrt{(\tilde{m}_0)_{22}/2}v = 125$ GeV. Different from the scenario in [1], in this paper, the dominant component for the 125 GeV scalar should be CP even so that there exists a SM limit for its couplings, while for the lightest scalar η, to the leading order of $(t_\beta s_\xi)$, we have

[5] We can always perform a global phase redefinition for ϕ_1 and ϕ_2 to keep one of the VEVs real, just like the case in (7).

[6] For the calculations in details, please see the Appendix. B in our recent paper [1], with the same conventions as those in this paper.

$$m_\eta^2 = \frac{v^2 t_\beta^2 s_\xi^2}{2}\left((\tilde{m}_2)_{11} - \frac{(\tilde{m}_1)_{12}^2}{(\tilde{m}_0)_{22}} - \frac{(\tilde{m}_1)_{13}^2}{(\tilde{m}_0)_{33}}\right)$$
$$= \frac{v^2 t_\beta^2 s_\xi^2}{2}\left[4\lambda_6 + 2\lambda_5(\lambda_3+\lambda_7)s_{2\theta}\left(\frac{1}{(\tilde{m}_0)_{22}} - \frac{1}{(\tilde{m}_0)_{33}}\right) - 4(\lambda_3+\lambda_7)^2\left(\frac{c_\theta^2}{(\tilde{m}_0)_{22}} + \frac{s_\theta^2}{(\tilde{m}_0)_{33}}\right) - \lambda_5^2\left(\frac{s_\theta^2}{(\tilde{m}_0)_{22}} + \frac{c_\theta^2}{(\tilde{m}_0)_{33}}\right)\right]; \tag{21}$$

$$\eta = I_2 - t_\beta s_\xi\left(\frac{(\tilde{m}_1)_{12}}{(\tilde{m}_0)_{22}}(c_\theta R_1 + s_\theta R_2) + \frac{(\tilde{m}_1)_{13}}{(\tilde{m}_0)_{33}}(c_\theta R_2 - s_\theta R_1) + \frac{I_1}{t_\xi}\right)$$
$$= I_2 - t_\beta s_\xi\left[\left(2(\lambda_3+\lambda_7)\left(\frac{c_\theta^2}{(\tilde{m}_0)_{22}} + \frac{s_\theta^2}{(\tilde{m}_0)_{33}}\right) + \frac{\lambda_5 s_{2\theta}}{2}\left(\frac{1}{(\tilde{m}_0)_{22}} - \frac{1}{(\tilde{m}_0)_{33}}\right)\right)R_1\right.$$
$$\left. + \left((\lambda_3+\lambda_7)s_{2\theta}\left(\frac{1}{(\tilde{m}_0)_{22}} - \frac{1}{(\tilde{m}_0)_{33}}\right) + \lambda_5\left(\frac{s_\theta^2}{(\tilde{m}_0)_{22}} + \frac{c_\theta^2}{(\tilde{m}_0)_{33}}\right)\right)R_2 + \frac{I_1}{t_\xi}\right]. \tag{22}$$

Thus, in the limit $t_\beta s_\xi \to 0$, we have $m_\eta \propto t_\beta s_\xi \to 0$ and $\eta \to I_2$, which means that η behaves like a light pseudoscalar but it has a small CP-even component.

We can diagonalize the fermion mass matrixes as

$$V_{U,L} M_U V_{U,R}^\dagger = \begin{pmatrix} m_u & 0 & 0 \\ 0 & m_c & 0 \\ 0 & 0 & m_t \end{pmatrix}, \qquad V_{D,L} M_D V_{D,R}^\dagger = \begin{pmatrix} m_d & 0 & 0 \\ 0 & m_s & 0 \\ 0 & 0 & m_b \end{pmatrix} \tag{23}$$

in which, according to (8), the mass matrixes are

$$(M_U)_{ij} = \frac{v}{\sqrt{2}}((Y_{1u})_{ij}c_\beta + (Y_{2u})_{ij}s_\beta e^{-i\xi}), \qquad (M_D)_{ij} = \frac{v}{\sqrt{2}}((Y_{1d})_{ij}c_\beta + (Y_{2d})_{ij}s_\beta e^{i\xi}). \tag{24}$$

The CKM matrix $V_{\rm CKM} = V_{U,L}V_{D,L}^\dagger$ as usual. We can rewrite the Yukawa couplings (8) in the quark sector adopting the Cheng-Sher ansatz [40]

$$\mathcal{L}'_{\rm Yuk,Q} = -\sum_{f=U_i,D_i} m_f \bar{f}_L f_R\left(1 + \frac{c_\beta R_1 + s_\beta c_\xi R_2 + s_\beta s_\xi I_2}{v}\right)$$
$$- \sum_{i,j}\frac{\xi_{ij}^U\sqrt{m_i^U m_j^U}}{v}\bar{U}_{i,L}U_{j,R}((c_\beta R_2 - s_\beta c_\xi R_1 + s_\beta s_\xi I_1) - i(c_\beta I_2 - s_\beta c_\xi I_1 - s_\beta s_\xi R_1))$$
$$- \sum_{i,j}\frac{\xi_{ij}^D\sqrt{m_i^D m_j^D}}{v}\bar{D}_{i,L}D_{j,R}((c_\beta R_2 - s_\beta c_\xi R_1 + s_\beta s_\xi I_1) + i(c_\beta I_2 - s_\beta c_\xi I_1 - s_\beta s_\xi R_1))$$
$$- \sum_{i,j}\frac{\sqrt{2m_i^D m_j^D}}{v}\bar{U}_{i,L}(V_{\rm CKM}\cdot\xi^D)_{ij}D_{j,R}H^+ - \sum_{i,j}\frac{\sqrt{2m_i^U m_j^U}}{v}\bar{D}_{i,L}(V_{\rm CKM}^\dagger\cdot\xi^U)_{ij}U_{j,R}H^- + \text{H.c.} \tag{25}$$

Similarly, in the lepton sector

$$\mathcal{L}'_{\rm Yuk,\ell} = -\sum_\ell m_\ell \bar{\ell}_L \ell_R\left(1 + \frac{c_\beta R_1 + s_\beta c_\xi R_2 + s_\beta s_\xi I_2}{v}\right)$$
$$- \sum_{i,j}\frac{\xi_{ij}^\ell\sqrt{m_i^\ell m_j^\ell}}{v}\bar{\ell}_{i,L}\ell_{j,R}((c_\beta R_2 - s_\beta c_\xi R_1 + s_\beta s_\xi I_1) + i(c_\beta I_2 - s_\beta c_\xi I_1 - s_\beta s_\xi R_1))$$
$$- \sum_{i,j}\frac{\sqrt{2m_i^\ell m_j^\ell}}{v}\bar{\nu}_{i,L}(V_{\rm PMNS}\cdot\xi^\ell)_{ij}\ell_{j,R}H^+ + \text{H.c.} \tag{26}$$

Here $V_{\rm PMNS}$ is the lepton mixing matrix [41] and

$$\xi^{U}_{ij} = (V_{U,L})_{ik}(-s_\beta e^{i\xi}(Y_{1u})_{kl} + c_\beta (Y_{2u})_{kl})(V^\dagger_{U,R})_{lj}; \quad (27)$$

$$\xi^{D(\ell)}_{ij} = (V_{D(\ell),L})_{ik}(-s_\beta e^{-i\xi}(Y_{1d(\ell)})_{kl} + c_\beta (Y_{2d(\ell)})_{kl})(V^\dagger_{D(\ell),R})_{lj}. \quad (28)$$

The off-diagonal elements of $\xi^{U,D,\ell}_{ij}$ induce the flavor-changing processes at tree level. It was proved in [1] that in the $t_\beta s_\xi \to 0$ limit, all the four quantities m_η, $c_{\eta,V}$, K, $J \propto t_\beta s_\xi$ which means the correlation between the lightest scalar and smallness of CP violation.

In the scenario we discuss in this paper, there can be exotic Higgs decay channels $h \to \eta\eta$, $Z\eta$ induced by

$$\mathcal{L}_{\rm exo} = \frac{c_{h\eta} g}{2c_W}(h\partial_\mu\eta - \eta\partial_\mu h)Z^\mu - \frac{1}{2} g_{h\eta\eta} v h \eta^2. \quad (29)$$

It leads to the branching ratios

$$\mathrm{Br}(h \to Z\eta) = \frac{g^2 c^2_{h\eta} m^3_h}{64\pi m^2_W \Gamma_{h,\rm tot}} \mathcal{F}\left(\frac{m^2_Z}{m^2_h}, \frac{m^2_\eta}{m^2_h}\right); \quad (30)$$

$$\mathrm{Br}(h \to \eta\eta) = \frac{g^2_{h\eta\eta} v^2}{32\pi m_h \Gamma_{h,\rm tot}} \sqrt{1 - \frac{4m^2_\eta}{m^2_h}} \quad (31)$$

where $\mathcal{F}(x,y) = (1 + x^2 + y^2 - 2x - 2y - 2xy)^{3/2}$, g is the weak coupling constant and $c_W \equiv m_W/m_Z$. For the detail couplings, please see Sec. A in the Appendixes, in which all $c_{h,f}$ are defined as the ratio between the Higgs-$f\bar{f}$ couplings and those in the SM.

III. CONSTRAINTS FOR THIS SCENARIO BY RECENT DATA

Besides the 125 GeV Higgs boson (h), there are two extra neutral scalars and one of which is expected to be light in this scenario. For the lightest scalar η with its mass $m_\eta \sim \mathcal{O}(0.1-1)$ GeV, the BESIII [42], *BABAR* [43,44], and CMS [45] experiments gave strict constraints; thus, we will focus on the cases $m_\eta \sim \mathcal{O}(10)$ GeV. Type II 2HDM including a light scalar with mass (25–80) GeV is excluded [46] through the search for $\eta b\bar{b}$ associated production, while, in general, it is still allowed by collider data, as we will show below. The two extra scalars would face the constraints from the direct searches at the LEP and LHC. In the Lee model scenario, with a light particle η, the exotic decay channels $h \to \eta\eta, Z\eta$ will modify the total width and signal strengths for the 125 GeV Higgs boson so that we should also consider the constraints from the Higgs signal strengths.

In the Lee model, there is no additional discrete symmetry to forbid flavor-changing processes at the tree level, and there are also new origins for CP violation. Thus, it must face the constraints in flavor physics, including rare decays, meson mixing, etc. The electric dipole moments (EDM) for electron [47] and neutron [48] would also give strict constraints in many models with additional CP-violation sources [49] including the Lee model, so we must consider the EDM constraints here as well.

A. Direct searches for extra scalars

The LEP experiments [50–52] set strict constraints on this scenario through the $e^+e^- \to Z\eta$ and $e^+e^- \to h\eta$ associated production processes. For η with its mass (15–40) GeV, [50,51] gave $\sigma_{Z\eta}/\sigma_{\rm SM} \lesssim (1.5\text{–}4) \times 10^{-2}$ at 95% C.L. which meant

$$c_{\eta,V} \lesssim (0.12 - 0.2); \quad (32)$$

thus, $t_\beta s_\xi \lesssim 0.1$ in this scenario. At the same mass region for η, assuming both η and h decay to $b\bar{b}$ final states dominantly, [51,52] gave $c^2_{h\eta} \lesssim (0.2 - 0.3)$. According to (A15), $c_{H,V} = c_{h\eta}$; thus, $c_{H,V}$ should also be small. The results implied that $c_{h,V} \sim 1$; thus, the couplings of h should be SM-like.

The direct searches for a heavy Higgs boson at the LHC [53,54] excluded a SM Higgs boson in the mass region (145–1000) GeV at 95% C.L. A SM Higgs boson with its mass around v would decay to WW and ZZ final states dominantly with $\mathrm{Br}(H_{\rm SM} \to VV) \approx 1$ [55], while in the 2HDM it can be modified because of a suppressed HVV coupling and the existence of other decay channels like $H \to Z\eta$, $\eta\eta$, $h\eta$, and Zh (if $m_H > m_Z + m_h = 216$ GeV), hh (if $m_H > 2m_h = 250$ GeV), H^+H^- (if $m_H > 2m_\pm$). For a heavy scalar H, analytically the partial widths should be

$$\Gamma_H(VV) \approx c^2_{H,V}\Gamma_{H,\rm SM}; \quad (33)$$

$$\Gamma_H(\eta\eta) = \frac{g^2_{H\eta\eta} v^2}{32\pi m_H}\sqrt{1 - \frac{4m^2_\eta}{m^2_H}}; \quad (34)$$

$$\Gamma_H(Z\eta) = \frac{c^2_{h,V} m^3_H}{8\pi v^2}\mathcal{F}\left(\frac{m^2_\eta}{m^2_H}, \frac{m^2_Z}{m^2_H}\right). \quad (35)$$

The suppression in $\Gamma_H(VV)$ comes from small $c_{H,V}$, while $\Gamma_H(Z\eta) \propto c^2_{h,V}$ is not suppressed because h is SM-like and $c_{h,V} \sim 1$. According to CMS results [53] which gave the most strict constraint, for $m_H \sim (200\text{–}300)$ GeV, the 95% C.L. upper limit for the signal strength is[7]

$$\mu_H \equiv \frac{\sigma_H}{\sigma_{H,\rm SM}} \cdot \frac{\mathrm{Br}(H \to VV)}{\mathrm{Br}_{\rm SM}(H \to VV)} \lesssim (0.1 - 0.2). \quad (36)$$

[7]For a heavy Higgs boson, $\mathrm{Br}_{\rm SM}(H \to VV) \sim 1$ according to [55].

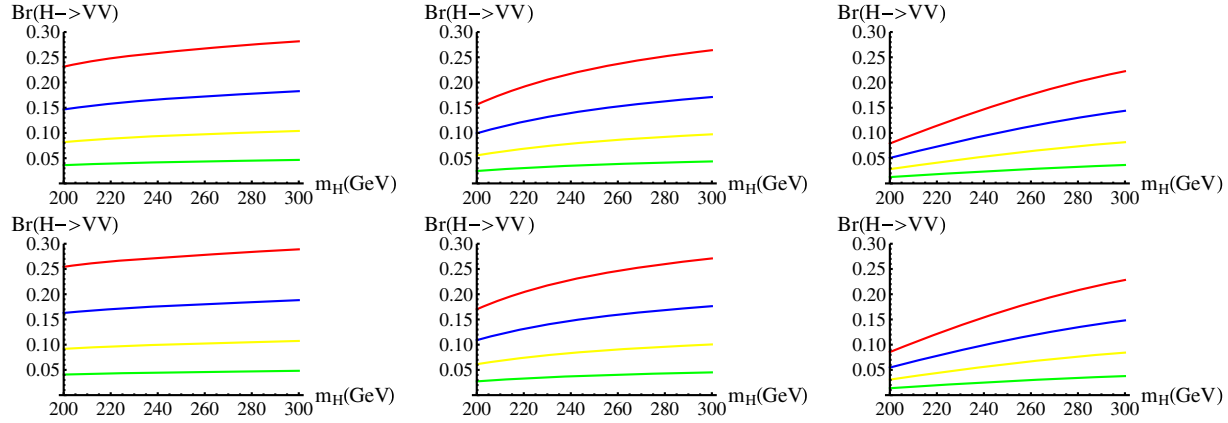

FIG. 1. $\mathrm{Br}(H \to VV) - m_H$ plots for different parameter choices fixing $c_{\eta,V} = 0.1$. The green, yellow, blue, and red lines stand for $c_{H,V} = 0.2$, 0.3, 0.4, 0.5, respectively, in each figure. The upper figures are for $m_\eta = 20$ GeV, while the lower figures are for $m_\eta = 40$ GeV. In each line, from left to right, we take $g_{H\eta\eta} = 0$, 0.5, 1.

Numerically, we show the $\mathrm{Br}(H \to VV) - m_H$ plots for different parameter choices fixing $c_{\eta,V} = 0.1$ in Fig. 1. From the figures, we can see that if the production cross section $\sigma_H \sim \sigma_{H,\mathrm{SM}}$, $c_{H,V} \lesssim 0.3$ would be allowed; while if $\sigma_H \sim 0.5\sigma_{H,\mathrm{SM}}$, $c_{H,V} \lesssim 0.4$ would also be allowed. It is not sensitive to m_η. We did not consider the $H \to hh$ channel for $m_H > 2m_h = 250$ GeV in the discussions above. Numerically, for $g_{Hhh} \sim 1$, we have $\mathrm{Br}(H \to hh) \lesssim 0.1$ which leads to $\sigma(pp \to H \to hh) \lesssim 0.4$ pb [55]. For this case, the direct search for $H \to hh$ channel by CMS [56] cannot give further constraint. We don't consider the case $m_H \gg v$ here because of the weakly coupled hypothesis.

No significant evidence for a charged Higgs boson had been found at colliders. Recently the ATLAS searches through $gb \to tH^-(\to \bar{t}b)$ process gave constraint on the $tbH^\pm$ vertex as [57]

$$|\xi_{tt}| \lesssim (1.5\text{–}3) \tag{37}$$

for a charged Higgs boson with mass $m_\pm$ in the region (200–600) GeV. In these searches, some hints for a charged Higgs signal with about 2.4σ significance were also found in this mass region. As can be seen below, it is consistent with this scenario.

B. Global-fits for Higgs signal strengths

The Higgs signal strength for a channel which exists in the SM is defined as

$$\mu_{i,f} \equiv \frac{\sigma \cdot \mathrm{Br}}{(\sigma \cdot \mathrm{Br})_{\mathrm{SM}}} = \frac{\sigma_i}{\sigma_{i,\mathrm{SM}}} \cdot \frac{\Gamma_h(f)}{\Gamma_{h,\mathrm{SM}}(f)} \cdot \frac{\Gamma_{h,\mathrm{tot,SM}}}{\Gamma_{h,\mathrm{tot}}}. \tag{38}$$

The SM Higgs boson with its mass $m_h = 125$ GeV has a total width $\Gamma_{h,\mathrm{tot,SM}} = 4.1$ MeV [55]. In this scenario, $\Gamma_{h,\mathrm{tot}}$ is also modified by the exotic decay channels $h \to Z\eta$, $\eta\eta$. Here for the VBF or Vh associated production channel, $\sigma/\sigma_{\mathrm{SM}} = c_{h,V}^2$, while for gluon fusion production,

$$\frac{\sigma}{\sigma_{\mathrm{SM}}} = \left| \mathrm{Re}(c_{h,t}) + \mathrm{i}\frac{\mathcal{B}_{1/2}(x_t)}{\mathcal{A}_{1/2}(x_t)} \mathrm{Im}(c_{h,t}) \right|^2. \tag{39}$$

For the decay channels $h \to WW^*$ and ZZ^*, we have $\Gamma_h(VV)/\Gamma_{h,\mathrm{SM}}(VV) = c_{h,V}^2$, for $h \to b\bar{b}$, $c\bar{c}$ and $\tau^+\tau^-$, $\Gamma_h(f)/\Gamma_{h,\mathrm{SM}}(f) = |c_{h,f}|^2$, and for the loop-induced decay processes,

$$\frac{\Gamma_h(gg)}{\Gamma_{h,\mathrm{SM}}(gg)} = \left| \mathrm{Re}(c_{h,t}) + \mathrm{i}\frac{\mathcal{B}_{1/2}(x_t)}{\mathcal{A}_{1/2}(x_t)} \mathrm{Im}(c_{h,t}) \right|^2, \tag{40}$$

$$\frac{\Gamma_h(\gamma\gamma)}{\Gamma_{h,\mathrm{SM}}(\gamma\gamma)} = \left| \frac{c_{h,V}\mathcal{A}_1(x_W) + \frac{4}{3}\mathrm{Re}(c_{h,t})\mathcal{A}_{1/2}(x_t) + (\frac{g_{h,\pm}v^2}{2m_\pm^2})\mathcal{A}_0(x_\pm) + \frac{4}{3}\mathrm{iIm}(c_{h,t})\mathcal{B}_{1/2}(x_t)}{\mathcal{A}_1(x_W) + \frac{4}{3}\mathcal{A}_{1/2}(x_t)} \right|^2. \tag{41}$$

Here $x_i \equiv m_h^2/4m_i^2$ where i denotes the particles t, W, or $H^\pm$ in loops. The index j in $\mathcal{A}(\mathcal{B})_j$ denotes the spin of the particle in loops; see the Feynman diagrams in Fig. 2. The analytical loop integration functions given by [58,59] are listed in Sec. B as (B1)–(B5). According to [55],

$$\Gamma_{h,\mathrm{tot}} = \Gamma_{h,\mathrm{tot,SM}}(0.58|c_{h,b}|^2 + 0.24c_{h,V}^2 + 0.06|c_{h,\tau}|^2 + 0.03|c_{h,c}|^2 + 0.09|c_{h,t}|^2(1 + 1.31\sin^2\alpha_t)) + \Gamma_{h,\mathrm{exo}} \tag{42}$$

where $\Gamma_{h,\mathrm{tot,SM}} = 4.1$ MeV for $m_h = 125$ GeV. $\alpha_t \equiv \arg(c_{h,t})$ and $\Gamma_{h,\mathrm{exo}}$ is the exotic decay width. Define

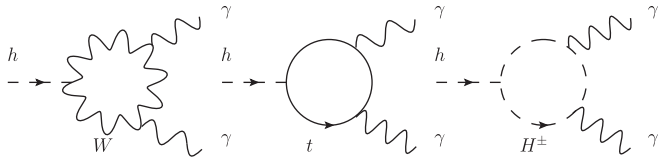

FIG. 2. Feynman diagrams for $h \to \gamma\gamma$ decay in this model.

$$\chi^2 \equiv \sum_{i,f} \left(\frac{\mu_{i,f,\mathrm{obs}} - \mu_{i,f,\mathrm{pre}}}{\sigma_{i,f}} \right)^2 \tag{43}$$

ignoring the correlations between different channels. $\mu_{i,f,\mathrm{obs(pre)}}$ means the observed (predicted) signal strength for production channel i and decay final state f and $\sigma_{i,f}$ means the standard deviation of the signal strength measurement for the corresponding channel. Numerically, the fitting results are not sensitive to the charged Higgs contribution in $h \to \gamma\gamma$ channel.

According to (A21), in this scenario, $c_{h,f} \sim 1$ holds for all fermions since h contains large component of R_1. Thus, for all $c_{h,f}$, the modifications from 1 are suppressed by t_β. We also have $c_{h,V} \sim 1$ in the text above. Thus, for any channel, according to (38),

$$\mu_{i,f,\mathrm{pre}} = \frac{\sigma_i}{\sigma_{i,\mathrm{SM}}} \cdot \frac{\Gamma_h(f)}{\Gamma_{h,\mathrm{SM}}(f)} \cdot \frac{\Gamma_{h,\mathrm{tot,SM}}}{\Gamma_{h,\mathrm{tot}}} \sim \frac{\Gamma_{h,\mathrm{tot,SM}}}{\Gamma_{h,\mathrm{tot}}}, \tag{44}$$

which means the signal strengths are mainly modified by the exotic decay width Γ_{exo}. Numerically, $\Gamma_{\mathrm{exo}} \lesssim$ (1–2) MeV is still allowed for other couplings close to those in SM. For $m_\eta < m_h/2$, the $h \to \eta\eta$ channel is available. And according to (31), we have

$$g_{h\eta\eta} \lesssim \mathcal{O}(10^{-2}), \tag{45}$$

which means a strong correlation among λ_i in the Higgs potential. To the leading order,

$$g_{h\eta\eta} = (\lambda_3 + \lambda_7) c_\theta + \frac{1}{2}\lambda_5 s_\theta + \mathcal{O}(t_\beta s_\xi), \tag{46}$$

which gives $\lambda_3 + \lambda_7 \simeq -\lambda_5 t_\theta/2 + \mathcal{O}(t_\beta s_\xi)$, while for $m_\eta < m_h - m_Z$, the $h \to Z\eta$ channel is open, and Eq. (30) gives

$$c_{H,V} = c_{h\eta} \lesssim \mathcal{O}(10^{-2} - 10^{-1}). \tag{47}$$

For $m_\eta \sim$ (15–30) GeV, $c_{h\eta} = 0.05$ is still allowed.

According to the direct searches for the heavy neutral Higgs boson H, we can see that $c_{H,V} = 0.3$ is in the allowed region for almost all cases. According to the bounds from the Higgs signal strengths, we can see for $m_\eta < m_h - m_Z = 34$ GeV, there would be further constraint on $c_{H,V}$ from the $h \to Z\eta$ rare decay channel. In this case, $c_{H,V} = 0.05$ would be allowed. Thus, we have two groups of typical benchmark points as listed in Table I. We choose $m_\eta = 20$ and 40 GeV as the two typical cases.

TABLE I. Benchmark points in the scalar sector for the following parts of this paper. The first line is a typical choice for the allowed case of $h \to Z\eta$ decay, while the second line is a typical choice for the forbidden case of $h \to Z\eta$ decay.

Case	m_η	m_H	$c_{h,f}$	$c_{\eta,V}$	$c_{H,V}$	$c_{h,V}$	$t_\beta s_\xi$
I	20 GeV	$\sim v$	~ 1	0.1	0.05	0.994	~ 0.1
II	40 GeV	$\sim v$	~ 1	0.1	0.3	0.95	~ 0.1

C. Constraints from oblique parameters

The GFitter group gave updated electroweak fitting results [60] for oblique parameters [61] as

$$S = 0.05 \pm 0.11, \quad T = 0.09 \pm 0.13, \quad U = 0.01 \pm 0.11,$$
$$R_{ST} = +0.90, \quad R_{SU} = -0.59, \quad R_{TU} = -0.83; \tag{48}$$

where R means the correlation between two variables. Here U is also treated as a free variable and the reference points are taken as $m_{h,\mathrm{ref}} = 125$ GeV, $m_{t,\mathrm{ref}} = 173$ GeV. In 2HDM, U is expected to be ignorable thus we can fix $U = 0$ and get [60]

$$S = 0.06 \pm 0.09, \qquad T = 0.10 \pm 0.07, \qquad R = +0.91. \tag{49}$$

In 2HDM, the contribution to δS and δT [3,62,63] are

$$\begin{aligned}\delta S = \frac{1}{24\pi}\Bigg[& (1-2s_W^2)^2 G(z_\pm, z_\pm) + c_1^2 G(z_2, z_3) + c_2^2 G(z_3, z_1) \\ & + c_3^2 G(z_1, z_2) + \sum_{i=1}^{3}\left(c_i^2 H(z_i) + \ln\left(\frac{m_i^2}{m_{H^\pm}^2}\right)\right) \\ & - H\left(\frac{m_{h,\mathrm{ref}}^2}{m_Z^2}\right) - \ln\left(\frac{m_{h,\mathrm{ref}}^2}{m_{H^\pm}^2}\right)\Bigg]; \end{aligned} \tag{50}$$

$$\begin{aligned}\delta T = \frac{1}{16\pi s_W^2 m_W^2}\Bigg[& \sum_{i=1}^{3}(1-c_i^2) F(m_{H^\pm}^2, m_i^2) - c_1^2 F(m_2^2, m_3^2) \\ & - c_2^2 F(m_3^3, m_1^2) - c_3^2 F(m_1^2, m_2^2) \\ & + 3\sum_{i=1}^{3} c_i^2 (F(m_Z^2, m_i^2) - F(m_W^2, m_i^2)) - 3(F(m_Z^2, m_{h,\mathrm{ref}}^2) \\ & - F(m_W^2, m_{h,\mathrm{ref}}^2))\Bigg]. \end{aligned} \tag{51}$$

The arguments above are defined as $z_i \equiv (m_i/m_Z)^2$ and $z_\pm \equiv (m_\pm/m_Z)^2$. The analytical loop integration functions given by [3,62,63] are listed in Sec. B as (B6)–(B9).

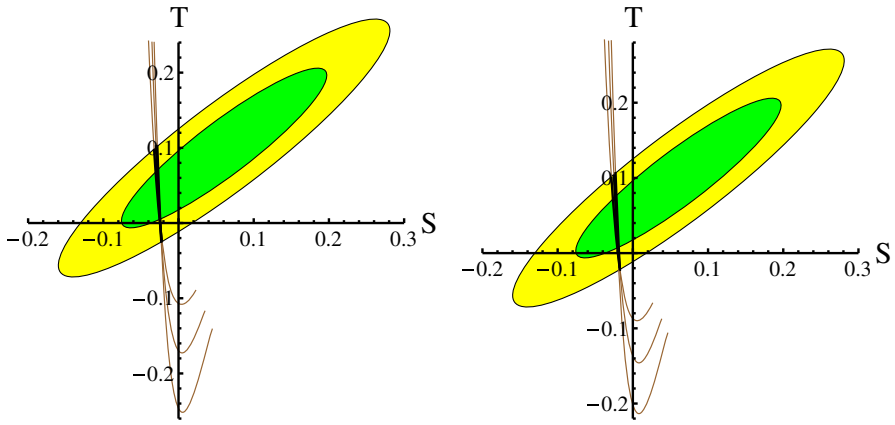

FIG. 3. Oblique parameter constraints for the scenario we discussed in this paper. The green region is 68% C.L. allowed and the yellow region is 95% C.L. allowed. The left figure is for case I, while the right figure is for case II in Table I. We plot the curves with a parameter $m_\pm$. In each curve, we begin with $m_\pm = 80$ GeV. In both figures, the curves from left to right are for $m_H = (200, 250, 300)$ GeV, respectively. For the allowed regions in the curves, we made them thick and black, please see the allowed regions in Table II in details.

We perform the fitting process based on the mathematica code [64][8] with the benchmark points in Table I. We plot the curves using the charged Higgs mass $m_\pm$ as a parameter in Fig. 3. Direct searches by LEP gave constraints on the charged Higgs boson mass as $m_\pm > 78.6$ GeV [65] at 95% C.L. so that we begin from $m_\pm = 80$ GeV. The thick regions in the curves stands for allowed regions by oblique parameter constrains for both benchmark points. For both cases in Table I, we list the allowed $m_\pm$ in Table II. For all the cases, allowed $m_\pm$ are around the heavy neutral Higgs mass m_H, as the scenario discussed by [16,66]. For m_H around the electroweak scale v, a charged Higgs boson should also have its mass around that scale. A light charged Higgs boson (with its mass $m_\pm < m_t$) is disfavored here; thus, we don't consider the constraints from the rare decay process $t \to H^+ b$.

D. Constraints from meson mixing data

The neutral mesons K^0, D^0, B^0, and B_s^0 should mix with their antiparticles through $W^\pm$ mediated box diagrams in the SM. Thus, a nontrivial contribution to $\langle \bar{M}^0|\mathcal{H}|M^0\rangle$ leads to the mass splitting effect between different CP eigenstates for the meson.[9] Here we list the experimental data [29,67] and SM predictions [68–71][10] for meson mixing in Table III, where the decay constants and bag parameters are from lattice data [72].

In general, we can parametrize the off-diagonal element in the mass matrix as [73,74]

$$\mathbf{m}_{12,M} \equiv \frac{1}{2m_M}\langle \bar{M}^0|\mathcal{H}|M^0\rangle = \mathbf{m}_{12,M}^{\mathrm{SM}}(1 + \Delta_M e^{2i\delta_M}), \quad (52)$$

where the factor $(2m_M)^{-1}$ comes from the normalization condition. In the SM, we must have $\Delta_M = \delta_M = 0$. In the $B^0(B_s^0)$ system, $\Delta m_{B(B_s)} = 2|\mathbf{m}_{12,B(B_s)}|$, while in the K^0 system, $\Delta m_K = 2\mathrm{Re}(\mathbf{m}_{12,K})$. A nonzero δ_M would also modify the CP-violation effects from those in SM. In the Lee model, the additional contributions to $\mathbf{m}_{12,M}$ are shown in Fig. 4. The neutral scalars $\phi = \eta$, h, H in the diagrams.

First, consider the left diagram in Fig. 4 which induce the mixing directly at tree level. It can contribute to the mixing of all the four kinds of mesons. The dominant contribution must come from η because it is light and its flavor-changing couplings are not suppressed by $t_\beta s_\xi$ or s_θ. The tree level η induced contribution for $M^0(f_i\bar{f}_j) - \bar{M}^0(f_j\bar{f}_i)$ mixing is [75,76]

TABLE II. Allowed regions for $m_\pm$ for each case above.

m_H (GeV)	200	250	300
Allowed $m_\pm$ for case I (GeV)	190–231	242–277	293–323
Allowed $m_\pm$ for case II (GeV)	185–228	232–269	279–311

TABLE III. Experimental data and SM predictions for mass splitting effects in meson mixing.

Meson	Δm_{exp} (GeV)	Δm_{SM} (GeV)
$K^0(d\bar{s})$	$(3.483 \pm 0.006) \times 10^{-15}$	$(3.30 \pm 0.34) \times 10^{-15}$
$D^0(c\bar{u})$	$(5.9 \pm 2.6) \times 10^{-15}$	⋯
$B_d^0(d\bar{b})$	$(3.36 \pm 0.02) \times 10^{-13}$	$(3.57 \pm 0.60) \times 10^{-13}$
$B_s^0(s\bar{b})$	$(1.1686 \pm 0.0014) \times 10^{-11}$	$(1.14 \pm 0.17) \times 10^{-11}$

[8]The second χ^2 (for 95% C.L.) should be 6.0 according to [29].

[9]In fact, in the real world, CP is not a good symmetry; thus, a mass eigenstate is modified a little from a CP eigenstate. See the details for this formalism in Sec. C.

[10]No SM prediction results for Δm_D appear because the dominant contribution comes from long-distance interactions; thus, it is difficult to calculate.

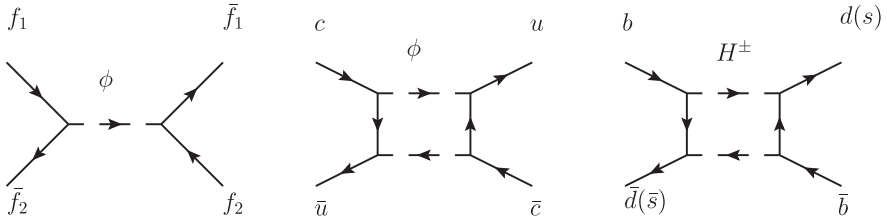

FIG. 4. Additional Feynman diagrams contributed to $\mathbf{m}_{12,M}$ in the Lee model.

$$\mathbf{m}_{12,M}^{\eta,\text{tree}} = \frac{f_M^2 B_M m_M m_i m_j}{12 m_\eta^2 v^2}\left[\left(1+\frac{6m_M^2}{(m_i+m_j)^2}\right)c_{\eta,ij}c_{\eta,ji}^* - \frac{5m_M^2}{2(m_i+m_j)^2}(c_{\eta,ij}^2 + c_{\eta,ji}^{*2})\right]. \tag{53}$$

Here f_M and B_M are the decay constant and bag parameter for meson M^0 separately. According to (A23), $c_{\eta,ij} = \pm\xi_{ij}(1+\mathcal{O}(t_\beta s_\xi))$. With the experimental constraints in [74,77], for different $\delta_{B(B_s)}$, $\Delta_{B(B_s)} \lesssim (0.1\text{–}0.4)$ at 95% C.L. Assuming $|\xi_{ij}| \sim |\xi_{ji}|$, numerically for $m_\eta \sim (20\text{–}40)$ GeV, we have

$$\begin{aligned} |\xi_{bd(db)}| &\lesssim (0.7\text{–}3)\times 10^{-2}, \\ |\xi_{bs(sb)}| &\lesssim (0.9\text{–}2.5)\times 10^{-2}. \end{aligned} \tag{54}$$

Similarly, $|\xi_{sd(ds)}| \lesssim (0.8\text{–}1.7)\times 10^{-2}$ for $K^0-\bar{K}^0$ mixing from [74], while for $D^0-\bar{D}^0$ mixing, we have $|\xi_{cu(uc)}| \lesssim (1.7\text{–}3.4)\times 10^{-2}$. For all four types of mixing, the constraints on ξ_{ij} are of $\mathcal{O}(10^{-2})$.

Next, consider the middle diagram in Fig. 4 which can induce a $D^0-\bar{D}^0$ mixing through top quark and a scalar mediated in the box. Assuming $|\xi_{tu(c)}| \sim |\xi_{u(c)t}|$, its contribution to Δm_D is [78]

$$\Delta m_D^{\eta,\text{box}} \approx \frac{m_u m_c |\xi_{tu}\xi_{tc}|^2}{24\pi^2 v^4} f_D^2 m_D B_D r \mathcal{F}_0\left(\frac{m_t^2}{m_\eta^2}\right), \tag{55}$$

where $r = (\alpha_s(m_t)/\alpha_s(m_b))^{6/23}(\alpha_s(m_b)/\alpha_s(m_c))^{6/25} = 0.8$ describes the QCD effects and loop function $\mathcal{F}_0(x)$ [78] is listed as (B10) in Sec. B in the Appendixes. Assuming its contribution is less than the complete Δm_D, numerically we have

$$|\xi_{tu}\xi_{tc}| \lesssim 6 \tag{56}$$

for a η with its mass (20–40) GeV.

Last, consider the right diagram in Fig. 4 which induce $B^0(B_s^0)-\bar{B}^0(\bar{B}_s^0)$ mixing through the box diagram in which one or two $W^\pm$ should be replaced by $H^\pm$ comparing with the case in SM. This kind of diagrams are highly suppressed in $K^0-\bar{K}^0$ mixing. In neutral B sector, the contributions from $W^\pm-H^\pm$ box and $H^\pm$ box can be estimated as [79]

$$\Delta_{B(B_s)}e^{i\delta_{B(B_s)}} = \xi_{tt}^2 \cdot \frac{\mathcal{F}_1(m_t^2/m_W^2, m_t^2/m_\pm^2, m_\pm^2/m_W^2) + \xi_{tt}^2\mathcal{F}_0(m_t^2/m_\pm^2)}{\mathcal{F}_2(m_t^2/m_W^2)}. \tag{57}$$

The loop functions $\mathcal{F}_i$ [79] are listed as (B10)–(B12) in Sec. B in the Appendixes, and $\mathcal{F}_0$ is the same as that in the box diagram for $D^0-\bar{D}^0$ mixing in (55). It is sensitive only to ξ_{tt} because the other terms are suppressed by the mass of down-type quarks. The S-T parameter fits favor a charged Higgs boson with mass $m_\pm \sim m_H \sim v$ (see also Table II), so numerically we have

$$|\xi_{tt}| \lesssim (0.6\text{–}0.9) \tag{58}$$

using the $B^0(B_s^0)-\bar{B}^0(\bar{B}_s^0)$ mixing constraints [74,77]. This bound is stricter than that from the direct searches for a charged Higgs boson in (37).

E. LHC constraints on top quark flavor violation

The ϕtq (where $q = c$, u and $\phi = \eta$, h) direct interactions in (A23) and (A24) would induce $t \to \phi q$ rare decay processes. The partial widths can be given by

$$\Gamma(t\to\phi q) = \frac{m_t^2 m_q(|c_{\phi,tq}|^2+|c_{\phi,qt}|^2)}{32\pi v^2}\left(1-\frac{m_\phi^2}{m_t^2}\right)^2. \tag{59}$$

For $\phi = \eta$, we have $c_{\eta,ij} = i\xi_{ij} + \mathcal{O}(t_\beta s_\xi) \sim i\xi_{ij}$, while for $\phi = h$, if $m_\eta < 34$ GeV, $c_{h,ij} \sim -it_\beta s_\xi \xi_{ij} \sim -0.1i\xi_{ij}$ with $t_\beta s_\xi \sim 0.1$; else $c_{h,ij} \sim (-0.1i + \mathcal{O}(0.1))\xi_{ij}$. For the latter case,

$$|c_{h,ij}| \sim (0.1\text{–}0.3)|\xi_{ij}|. \tag{60}$$

All the numerical estimations above are based on (A23) and (A24) etc. in Sec. A. The combined experimental result by ATLAS [80] gave

$$\text{Br}(t\to hc) < 0.46\% \quad \text{and} \quad \text{Br}(t\to hu) < 0.45\%, \tag{61}$$

respectively, at 95% C.L. Assuming $|\xi_{ij}| \sim |\xi_{ji}|$ as usual, we have

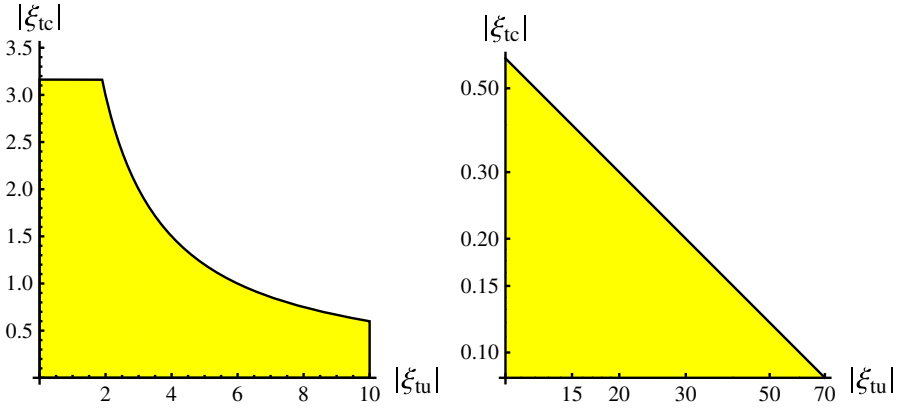

FIG. 5. Allowed region for top flavor-changing couplings. Notice in the right figure we used double-log coordinates to show a very large region.

$$|\xi_{tu}| \lesssim (1\text{–}3) \times 10^2 \quad \text{and} \quad |\xi_{tc}| \lesssim (5\text{–}14), \tag{62}$$

using the SM predicted top quark total width $\Gamma_{t,\mathrm{tot}} \approx 1.3$ GeV [29,81].

It is difficult to search for $t \to \eta q$ rare decay since η decays to jets dominantly, but we can obtain the constraints through the exotic decay branching ratio of top quark. The $t\bar{t}$ production cross section measurements at the LHC with $\sqrt{s} = 8$ TeV gave $\sigma_{t\bar{t}} = (237 \pm 13)$ pb [82] assuming $m_t = 173$ GeV and $\mathrm{Br}(t \to Wb) = 1$, which is consistent with the SM prediction $\sigma_{t\bar{t},\mathrm{SM}} = (246^{+9}_{-11})$ pb [83]. Thus, we have for the top exotic decay channels that $\Gamma(t \to \text{exotic})/\Gamma(t \to Wb) < 8\%$ at 95% C.L. In this scenario, $\mathrm{Br}(t \to \eta q)/\mathrm{Br}(t \to hq) \sim \mathcal{O}(10\text{–}10^2)$; thus, $t \to hq$ can be ignored in this paragraph. With these data, we have

$$2 \times 10^{-4}|\xi_{tu}|^2 + 0.1|\xi_{tc}|^2 \lesssim 1 \tag{63}$$

for $m_\eta \sim (20\text{–}40)$ GeV.

The last constraint comes from same-sign top production. The 95% C.L. upper limit given by CMS [84] is $\sigma_{tt} < 0.37$ pb. Theoretically, η mediated $uu \to tt$ process would be the dominant production channel in this scenario. The cross section can be expressed as

$$\sigma(uu \to tt) = \int dx_1 dx_2 f_u(x_1) f_u(x_2) \sigma(s_0), \tag{64}$$

where $f_u(x)$ is the parton distribution function (PDF) for up quark and

$$\begin{aligned}\sigma(s_0) = {} & \frac{m_u^2 m_t^2 \beta_t (|\xi_{tu}|^2 + |\xi_{ut}|^2)^2}{64\pi s_0 v^4} \\ & \times \int_{-1}^{1} dc_\theta \left[\left(\frac{1 - \beta_t c_\theta}{1 + \beta_t^2 + 4m_\eta^2/s_0 - 2\beta_t c_\theta} \right)^2 \right. \\ & \times \left(\frac{1 + \beta_t c_\theta}{1 + \beta_t^2 + 4m_\eta^2/s_0 + 2\beta_t c_\theta} \right)^2 \\ & \left. - \frac{1 + \beta_t^2 (c_\theta^2 - 2)}{(1 + \beta_t^2 + 4m_\eta^2/s_0)^2 - 4\beta_t^2 c_\theta^2} \right].\end{aligned} \tag{65}$$

Here $s_0 \equiv x_1 x_2 s_{\mathrm{LHC}}$ is the square of energy in the moment center frame of two partons, $\beta_t \equiv \sqrt{1 - 4m_t^2/s_0}$ is the velocity of the top quark, and θ is the azimuth angle of the top quark in respect to the beam line. Numerically, for $m_\eta \sim (20\text{–}40)$ GeV, assuming $|\xi_{tu}| \sim |\xi_{ut}|$ and using the MSTW2008 PDF [85], we have

$$|\xi_{tu}| \lesssim 10^2. \tag{66}$$

Combining the equations (56), (62), (63), and (66), we plot the estimations of allowed region in the $|\xi_{tu}| - |\xi_{tc}|$ plane in Fig. 5. The strictest upper limit $|\xi_{tc}| \lesssim 3$ and $|\xi_{tu}| \lesssim 70$ comes from (63), and the obvious behavior of the correlation between $|\xi_{tc}|$ and $|\xi_{tu}|$ comes from (56). The boundary contains relative errors of $\mathcal{O}(10\%)$ and it is not sensitive to m_η for $m_\eta \sim (20\text{–}40)$ GeV.

F. Constraints on lepton flavor violation

In type III 2HDM [37] there exist direct $\ell_i \ell_j \phi$ vertices to be constrained. For the discovered 125 GeV Higgs boson, a straightforward calculation gives [86]

$$\mathrm{Br}(h \to \ell_i^{\pm} \ell_j^{\mp}) = \frac{m_h m_i m_j}{8\pi \Gamma_h v^2} (|c_{h,ij}|^2 + |c_{h,ji}|^2). \tag{67}$$

For $h \to \mu\tau$ process, direct searches by CMS [86] and ATLAS [87] collaborations gave $\mathrm{Br}(h \to \mu\tau) < 1.51\%$ and $\mathrm{Br}(h \to \mu\tau) < 1.85\%$, respectively, both at 95% C.L.[11] In this scenario, $|c_{h,ij}|$ is suppressed to be $(0.1\text{–}0.3)|\xi_{ij}|$ for $m_\eta \sim (20\text{–}40)$ GeV, assuming $|c_{h,ij}| \sim |c_{h,ji}|$, we have the bound

$$|\xi_{\mu\tau}| \lesssim (5\text{–}16). \tag{68}$$

[11] Especially for the $h \to \mu\tau$ signal, the CMS result gave a 2.4σ hint corresponding to the best-fit branching ratio $\mathrm{Br}(h \to \mu\tau) = (0.84^{+0.39}_{-0.37})\%$ [86].

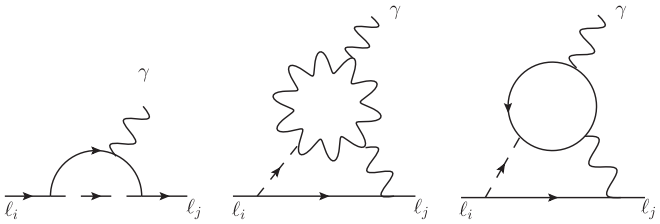

FIG. 6. Feynman diagrams contributed to radiative LFV decays $\ell_i \to \ell_j\gamma$.

Another kind of strict constraint on the $\ell_i\ell_j\phi$ vertices comes from radiative LFV decays as $\tau \to \mu\gamma$ and $\mu \to e\gamma$. For $\tau \to \mu(e)\gamma$, Belle and *BABAR* collaborations gave the 90% C.L. upper limit as [88,89]

$$\begin{aligned} &\mathrm{Br}(\tau \to \mu\gamma) < 4.5 \times 10^{-8}, \\ &\mathrm{Br}(\tau \to e\gamma) < 1.2 \times 10^{-7}\ \text{(Belle)}; \end{aligned} \tag{69}$$

$$\begin{aligned} &\mathrm{Br}(\tau \to \mu\gamma) < 4.4 \times 10^{-8}, \\ &\mathrm{Br}(\tau \to e\gamma) < 3.3 \times 10^{-8}\ (BABAR), \end{aligned} \tag{70}$$

while for $\mu \to e\gamma$, the MEG Collaboration gave [90]

$$\mathrm{Br}(\mu \to e\gamma) < 5.7 \times 10^{-13} \tag{71}$$

at 90% C.L. In the SM, the branching ratios of $\ell_i \to \ell_j\gamma$ processes are estimated to be of $\mathcal{O}(10^{-56}$–$10^{-54})$ [29,91,92] which are far below the experimental sensitivity. But in 2HDM with LFV, it can be larger or even comparable to recent data. In this model, $\ell_i \to \ell_j\gamma$ process can be generated by Feynman diagrams in Fig. 6, and the branching ratios can be expressed as [93]

$$\frac{\mathrm{Br}(\ell_i \to \ell_j\gamma)}{\mathrm{Br}(\ell_i \to \ell_j\nu_i\bar{\nu}_j)} = \frac{48\pi^3\alpha}{G_F^2}(|A_L|^2 + |A_R|^2), \tag{72}$$

where $A_{L(R)}$ are defined through [94,95]

$$\begin{aligned} &\mathcal{M}(\ell_i \to \ell_j\gamma) \\ &\quad = em_i\bar{u}_j(p_j)\mathrm{i}\sigma^{\mu\nu}q_\nu(A_LP_L + A_RP_R)u_i(p_i)\epsilon_\mu^*(q) \end{aligned} \tag{73}$$

in which $P_{L(R)} \equiv (1 \mp \gamma^5)/2$ and q is the momentum of the photon. According to Fig. 6, there are one-loop and two-loop contributions to these processes where the two-loop diagrams are called Barr-Zee-type diagrams [96].[12] For $\tau \to \mu(e)\gamma$, the analytical expression for left-handed (right-handed) amplitude should be [92–95,97,98][13]

$$\begin{aligned} A_L^*(A_R) &= A_{L,\text{one-loop}}^*(A_{R,\text{one-loop}}) + A_{L,\text{two-loop}}^*(A_{R,\text{two-loop}}) \\ &= \sum_\phi \frac{\sqrt{m_im_j}c_{\phi,ij}(c_{\phi,ji})}{16\pi^2v^2}\left(\frac{m_i}{m_h^2}\left(c_{\phi,i}\ln\left(\frac{m_h^2}{m_i^2}\right) - \frac{4}{3}|c_{\phi,i}|\cos(\alpha_{\phi,i}) - \frac{5}{3}\mathrm{i}|c_{\phi,i}|\sin(\alpha_{\phi,i})\right)\right. \\ &\quad + \frac{c_{\phi,V}\alpha}{\pi m_i}\left(\left(3 + \frac{m_\phi^2}{2m_W^2}\right)f\left(\frac{m_W^2}{m_\phi^2}\right) + \left(\frac{23}{4} - \frac{m_\phi^2}{2m_W^2}\right)g\left(\frac{m_W^2}{m_\phi^2}\right) + \frac{3}{4}h\left(\frac{m_W^2}{m_\phi^2}\right)\right) \\ &\quad \left. - \frac{8\alpha|c_{\phi,t}|}{3\pi m_i}\left(\cos(\alpha_{\phi,t})f\left(\frac{m_t^2}{m_\phi^2}\right) + \mathrm{i}\sin(\alpha_{\phi,t})g\left(\frac{m_t^2}{m_\phi^2}\right)\right)\right), \end{aligned} \tag{74}$$

where $i = \tau$, $j = e$, μ, $\alpha_{\phi,f} \equiv \arg(c_{\phi,f})$ and the loop integration functions f, g, h [93,97] are listed in (B13)–(B15) in Sec. B. Numerically, the loop contributions with a charged Higgs or Z boson inside are both small; thus, we ignore them. However, for the $\mu \to e\gamma$ decay, which means $i = \mu$ and $j = e$, the one-loop contribution should be changed to

$$A_{L,\text{one-loop}}^{*(\mu\to e\gamma)} = \sqrt{\frac{m_e}{m_\mu}}\sum_\phi \frac{m_\tau^2c_{\phi,\tau e}c_{\phi,\mu\tau}}{16\pi^2m_\phi^2v^2}\left(\ln\left(\frac{m_\phi^2}{m_\tau^2}\right) - \frac{3}{2}\right) \tag{75}$$

because the loop with τ inside is expected to give a larger contribution compared with the μ case when adopting the Cheng-Sher ansatz [40]. For A_R, we should take $c_{\phi,e\tau}c_{\phi,\tau\mu}$ instead of $c_{\phi,\tau e}c_{\phi,\mu\tau}$ in A_L^*.

Numerically, we take the benchmark points as those in Table I. For $m_\eta = 20$ GeV,

[12]This kind of two-loop diagram was first used by Barr and Zee to calculate the electric dipole moments for fermions in [96] which will also be discussed later.

[13]Notice that the analytical formulas for the $\ell_i \to \ell_j\gamma$ decay process in these papers are not consistent with each other. We checked the calculation during completion of our recent paper [92] and confirmed that the result by Omura *et al.* [94,95] is correct.

$$\mathrm{Br}(\tau \to \mu\gamma) \simeq 1.7 \times 10^{-10}(|\xi_{\tau\mu}|^2 + |\xi_{\mu\tau}|^2)| - 5.7\xi_{\tau\tau} - 5.4\xi_{tt} + 1.2\mathrm{i}|^2; \quad (76)$$

$$\mathrm{Br}(\tau \to e\gamma) \simeq 8.4 \times 10^{-13}(|\xi_{\tau e}|^2 + |\xi_{e\tau}|^2)| - 5.7\xi_{\tau\tau} - 5.4\xi_{tt} + 1.2\mathrm{i}|^2. \quad (77)$$

We used $\mathrm{Br}(\tau \to e\nu_\tau\bar{\nu}_e) = 17.8\%$ and $\mathrm{Br}(\tau \to \mu\nu_\tau\bar{\nu}_\mu) = 17.4\%$ [29] in the calculations above. For a typical case, $|\xi_{\mu(e)\tau}| \sim |\xi_{\tau\mu(e)}|$, $\xi_{tt} \sim 0.6$, and $\xi_{\tau\tau} \sim 1$, we have $\mathrm{Br}(\tau \to \mu\gamma) \sim 3 \times 10^{-8}|\xi_{\mu\tau}|^2$; thus, the upper limit for $|\xi_{\mu\tau}|$ should be around 1. For $\mathrm{Br}(\tau \to e\gamma) \sim 10^{-10}|\xi_{e\tau}|^2$, $|\xi_{e\tau}| \sim \mathcal{O}(10)$ is still allowed. For $m_\eta = 40$ GeV,

$$\mathrm{Br}(\tau \to \mu\gamma) \simeq 1.7 \times 10^{-10}(|\xi_{\tau\mu}|^2 + |\xi_{\mu\tau}|^2)| - 2\xi_{\tau\tau} - 2.5\xi_{tt} - 0.3 + \mathrm{i}|^2; \quad (78)$$

$$\mathrm{Br}(\tau \to e\gamma) \simeq 8.4 \times 10^{-13}(|\xi_{\tau e}|^2 + |\xi_{e\tau}|^2)| - 2\xi_{\tau\tau} - 2.5\xi_{tt} - 0.3 + \mathrm{i}|^2. \quad (79)$$

Choosing the same parameters as above, $\mathrm{Br}(\tau \to \mu\gamma) \sim 5 \times 10^{-9}|\xi_{\mu\tau}|^2$ which gives the upper limit of $|\xi_{\mu\tau}|$ to be around 3, while for $\mathrm{Br}(\tau \to e\gamma) \sim 2 \times 10^{-11}|\xi_{e\tau}|^2$, $|\xi_{e\tau}| \sim \mathcal{O}(10\text{–}10^2)$ are allowed. In the discussions above, we assumed real $\xi_{tt(\tau\tau)}$. If $\xi_{tt(\tau\tau)}$ were complex, some accidental cancellation would make larger $|\xi_{\mu\tau}|$ possible.

For $\tau \to \mu\gamma$ decay, it poses a stricter constraint than that from $h \to \mu\tau$ decay in (68) with $m_\eta \sim (20\text{–}40)$ GeV. Different from the cases discussed in [92] in which the 125 GeV scalar is the lightest one, in this scenario, the one-loop contribution from (20–40) GeV light scalar would be dominant or at least comparable with the two-loop contributions. At the same time, $h\mu\tau$ vertex is suppressed by s_θ and $t_\beta s_\xi$ to be of $\mathcal{O}(0.1)$. So that in this scenario, $\tau \to \mu\gamma$ decay gives dominant constraint on the LFV vertex instead of $h \to \mu\tau$ decay. For $\tau \to e\gamma$ decay, $|\xi_{e\tau}|$ is constrained to be less than $\mathcal{O}(10\text{–}10^2)$ which is still away from the expected magnitude by Cheng-Sher ansatz.

Numerically, for the $\mu \to e\gamma$ decay, choosing typically $\xi_{ij} \sim \xi_{ji}$, we have

$$\mathrm{Br}(\mu \to e\gamma) = 5.7 \times 10^{-9}| - \xi_{e\tau}\xi_{\mu\tau} + \xi_{e\mu}(-0.9\xi_{tt} + 0.2\mathrm{i})|^2, \quad (m_\eta = 20\ \mathrm{GeV}); \quad (80)$$

$$\mathrm{Br}(\mu \to e\gamma) = 5.7 \times 10^{-11}| - 3.6\xi_{e\tau}\xi_{\mu\tau} + \xi_{e\mu}(-7.7\xi_{tt} + 1.6\mathrm{i})|^2, \quad (m_\eta = 40\ \mathrm{GeV}). \quad (81)$$

Choosing $|\xi_{tt}| \sim 0.6$ as usual, the three LFV couplings $\xi_{e\mu,e\tau,\mu\tau}$ are strongly correlated between each other. The typical upper limit for $|\xi_{e\mu}|$ and $|\xi_{e\tau}\xi_{\mu\tau}|$ are both of $\mathcal{O}(10^{-2})$ for $m_\eta \sim (20\text{–}40)$ GeV. For example, fixing $\xi_{e\tau} = 0$ (or $\xi_{\mu\tau} = 0$),

$$|\xi_{e\mu}| \lesssim (1.4\text{–}3.3) \times 10^{-2}, \quad (82)$$

while fixing $\xi_{e\mu} = 0$,

$$|\xi_{e\tau}\xi_{\mu\tau}| \lesssim (1.0\text{–}2.8) \times 10^{-2}. \quad (83)$$

G. Constraints from electric dipole moments

The effective interaction for EDM of a fermion f can be written as [49]

$$\mathcal{L}_{\mathrm{EDM}} = -\frac{\mathrm{i}}{2} d_f \bar{f}\sigma^{\mu\nu}\gamma^5 f F_{\mu\nu}, \quad (84)$$

which violates both P and CP symmetries. In the SM, the only origin of CP violation is the complex CKM matrix [25,26]; thus, the EDM for electrons and neutrons are generated at the four- and three-loop level, respectively, and they are estimated to be [49]

$$d_e \sim 10^{-38} e \cdot \mathrm{cm}, \quad \text{and} \quad d_n \sim 10^{-32} e \cdot \mathrm{cm}. \quad (85)$$

They are still far below the experimental upper limits [47,48],

$$|d_e| < 8.7 \times 10^{-29} e \cdot \mathrm{cm}, \quad \text{and} \quad |d_n| < 2.9 \times 10^{-26} e \cdot \mathrm{cm}, \quad (86)$$

both at 90% C.L. In the BSM with additional origins of CP violation, the EDM for a fermion might be generated at the one- or two-loop level[14]; thus, they can be quite a bit larger than those in the SM or even reach the sensitivity of recent data.

The EDM for a fermion f can be generated from the Feynman diagrams in Fig. 7 if there exists CP violation in $\phi f\bar{f}$ vertices. The two-loop diagrams are called Barr-Zee diagrams [96]. If there is no CP violation in flavor-changing vertices, the one-loop contributions are proportional to (m_f/v);[3] thus, they are usually negligible for light fermions. The dominant contributions come from the Barr-Zee diagram as [96,100–102]

$$\frac{d_f}{e} = \sum_\phi \frac{2\sqrt{2}\alpha_{\mathrm{em}} G_F Q_f m_f |c_{\phi,f}|}{(4\pi)^3} \times \left(\sin\alpha_{\phi,f}(c_{\phi,V}\mathcal{J}_1(m_W, m_\phi) + g_{\phi,\pm}\mathcal{J}_0(m_\pm, m_\phi)) - \frac{8}{3}|c_{\phi,t}|(\sin\alpha_{\phi,t}\cos\alpha_{\phi,f}\mathcal{J}_{1/2}(m_t, m_\phi) + \cos\alpha_{\phi,t}\sin\alpha_{\phi,f}\mathcal{J}'_{1/2}(m_t, m_\phi)) \right). \quad (87)$$

[14]Nonperturbation effects arising from the θ term may also give significant contributions to the neutron EDM [99], but we don't include that in this paper.

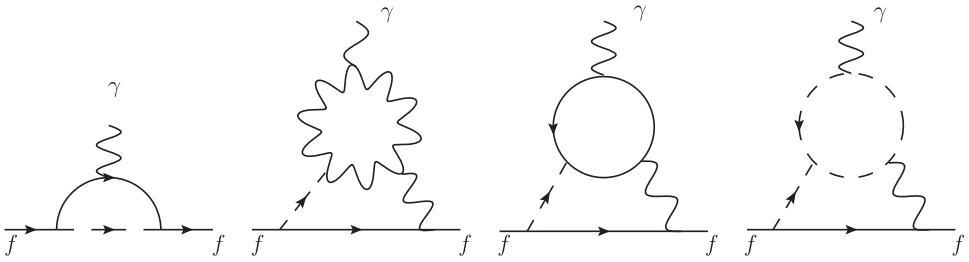

FIG. 7. Feynman diagrams contributed to EDM for a fermion f.

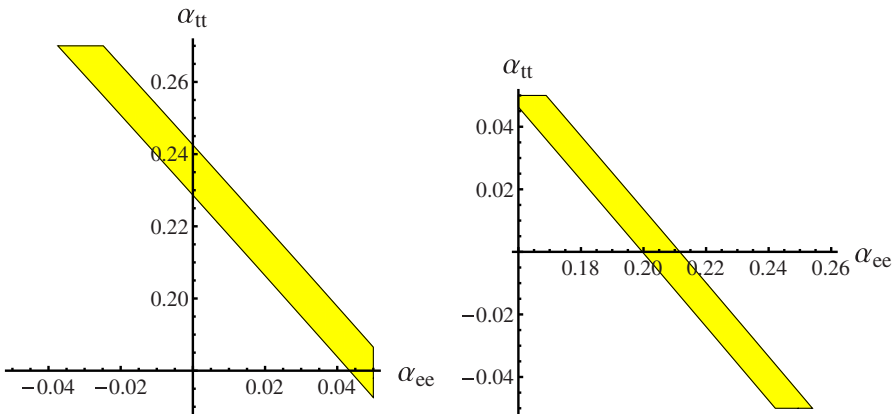

FIG. 8. Constraints in $\alpha_{ee} - \alpha_{tt}$ plane by electron EDM. Fix $m_\eta = 20$ GeV, $|\xi_{tt}| = 0.6$, and $\xi_{ee} = 1$. Yellow regions are allowed at 90% C.L, here and until Fig. 11.

Here Q_f is the electric charge for the fermion f, $\alpha_{\phi,f} \equiv \arg(c_{\phi,f})$, and the $\phi H^+ H^-$ vertex $g_{\phi,\pm} \equiv (1/v)(\partial^3 V/\partial\phi\partial H^+\partial H^-)$ is defined in (A10). The first term comes from the $W^\pm$-loop contribution (the second figure in Fig. 7), the second term comes from the $H^\pm$-loop contribution (the last figure in Fig. 7)[15], and the last two terms come from the top-loop contribution (the third figure in Fig. 7). The loop functions $\mathcal{J}_i$ [101] are all listed in Sec. B in (B16)–(B19).

For an electron, (87) can fully describe its EDM if we ignore the one-loop contributions. Numerically, we take the benchmark points as those in Table I and fix $|\xi_{tt}| = 0.6$ as usual. Precision measurement by [47] requires strong correlation among parameters to generate the cancellation between different contributions [1,103]. We define $\alpha_{ij} \equiv \arg(\xi_{ij})$ and show some allowed regions at 90% C.L. in Figs. 8–11 in the $\alpha_{ee} - \alpha_{tt}$ plane.

From the figures, we can see for fixing $|\xi_{ee,tt}|$, α_{tt} and α_{ee} have strong negative correlation. In Fig. 8 and Fig. 9, we both choose $m_\eta = 20$ GeV. For $|\xi_{ee}| = 1$, the allowed band is very narrow for $\Delta\alpha \sim 10^{-2}$, while for $|\xi_{ee}| = 0.3$, the allowed band is wider for $\Delta\alpha \sim (3\text{–}4) \times 10^{-2}$. In Fig. 10 and Fig. 11, we both choose $m_\eta = 40$ GeV. The behaviors are the same as the case $m_\eta = 20$ GeV, but the constraints are a bit weaker. For $|\xi_{ee}| = 1$, $\Delta\alpha \sim (1\text{–}2) \times 10^{-2}$; while for $|\xi_{ee}| = 0.3$, $\Delta\alpha \sim (5\text{–}7) \times 10^{-2}$. The charged Higgs loops give subdominant contributions, thus the final results are not sensitive to $\phi H^+ H^-$ couplings. The location of the allowed regions would shift a little bit for different choices of $\phi H^+ H^-$ couplings.

The one-loop contribution induced by flavor-diagonal interaction, shown as the first figure in Fig. 7, is estimated for election as $|d_e| \sim (e m_e^3/16\pi^2 v^2 m_\phi^2) \ln(m_\phi^2/m_e^2) \sim 10^{-32} e \cdot \text{cm}$ which is negligible small. The flavor-changing vertices should also generate CP-violation effects. If a τ runs in this loop, the one-loop contribution for d_e is [98,104,105]

$$\Delta d_e = -\sum_\phi \frac{e m_e m_\tau^2 |c_{\phi,e\tau}|^2 \sin(2\alpha_{\phi,e\tau})}{16\pi^2 v^2 m_\phi^2} \left(\ln\left(\frac{m_\phi^2}{m_\tau^2}\right) - \frac{3}{2} \right). \tag{88}$$

For $|\xi_{e\tau}| \lesssim 0.1$, the one-loop contribution is $|d_e| \lesssim 10^{-28} e \cdot \text{cm}$; thus, it is negligible compared with the recent experimental sensitivity [47]. While if $|\xi_{e\tau}|$

[15]Numerically, the charged Higgs contribution is small compared with $W^\pm$ or top contributions as usual, but it may be comparable with experimental data especially for electrons, so it is not negligible like that in radiative LFV decay calculations.

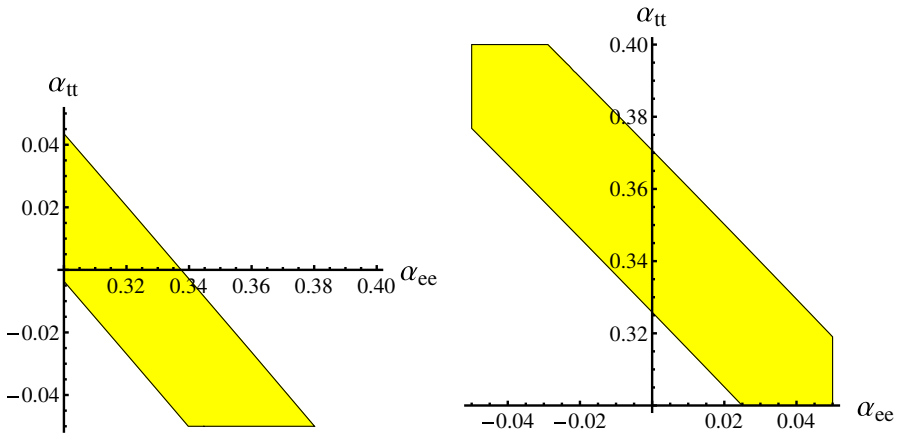

FIG. 9. Constraints in $\alpha_{ee} - \alpha_{tt}$ plane by electron EDM. Fix $m_\eta = 20$ GeV, $|\xi_{tt}| = 0.6$, and $\xi_{ee} = 0.3$.

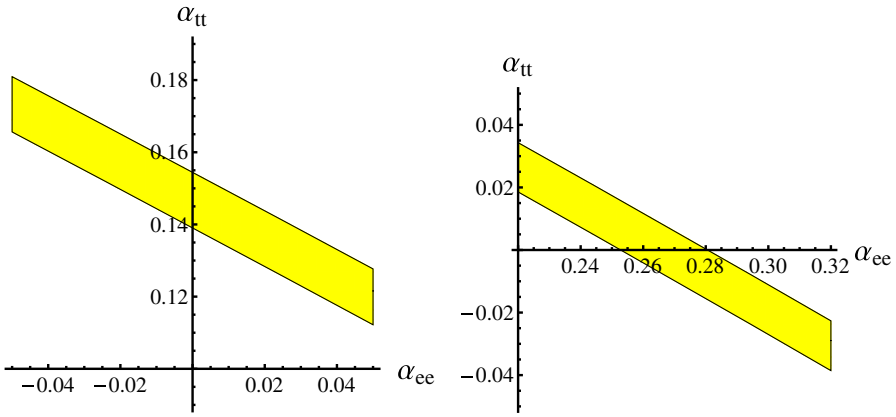

FIG. 10. Constraints in $\alpha_{ee} - \alpha_{tt}$ plane by electron EDM. Fix $m_\eta = 40$ GeV, $|\xi_{tt}| = 0.6$, and $\xi_{ee} = 1$.

is larger, for example, we can take $|\xi_{e\tau}| \sim \mathcal{O}(1)$,[16] and the one-loop contribution to $|d_e|$ would reach $\mathcal{O}(10^{-27}$–$10^{-26})e \cdot \mathrm{cm}$. In this case, the allowed region would be modified a little bit. As an example, for the parameters in Fig. 8, we show the allowed region before and after adding the one-loop contribution $\Delta d_e = \pm 10^{-27} e \cdot \mathrm{cm}$ in Fig. 12.

The neutron EDM contains four types of contribution [49], including quark EDM d_q, quark color EDM (CEDM) $\tilde{d}_q$, Weinberg operator [106,107] w, and the strong CP term [99] which would not be discussed in this paper. Thus, [49,100]

$$\frac{d_n}{e} \simeq 1.4\left(\frac{d_d}{e} - 0.25\frac{d_u}{e}\right) + 1.1(\tilde{d}_d + 0.5\tilde{d}_u) + (22\ \mathrm{MeV})w. \tag{89}$$

We ignore the CP-violation effects in flavor-changing vertices now. The EDM for u and d quarks are just those in (87) which come from the Barr-Zee-type contributions, and the CEDM from the Barr-Zee diagrams are given by [96,100]

$$\begin{aligned}\tilde{d}_q = -\sum_\phi \frac{2\sqrt{2}G_F\alpha_s m_q |c_{\phi,t}c_{\phi,q}|}{(4\pi)^3} \\ \times (\sin\alpha_{\phi,t}\cos\alpha_{\phi,q}\mathcal{J}_{1/2}(m_t, m_\phi) \\ + \cos\alpha_{\phi,t}\sin\alpha_{\phi,q}\mathcal{J}'_{1/2}(m_t, m_\phi)),\end{aligned} \tag{90}$$

where the loop functions are the same as those in (87). The contribution from the Weinberg operator is [100,106,107]

$$w = \sum_\phi \frac{\sqrt{2}G_F g_s \alpha_s |c_{\phi,t}|^2}{4\cdot(4\pi)^3}\sin\alpha_{\phi,t}\cos\alpha_{\phi,t}\mathcal{K}\left(\frac{m_t^2}{m_\phi^2}\right), \tag{91}$$

where the loop function $\mathcal{K}$ is listed in (B22) in Sec. B. Including the running effects for these operators as well (see the Appendixes in [100]),

[16]Which means $|\xi_{\mu\tau}| \lesssim \mathcal{O}(10^{-2})$ according to (83).

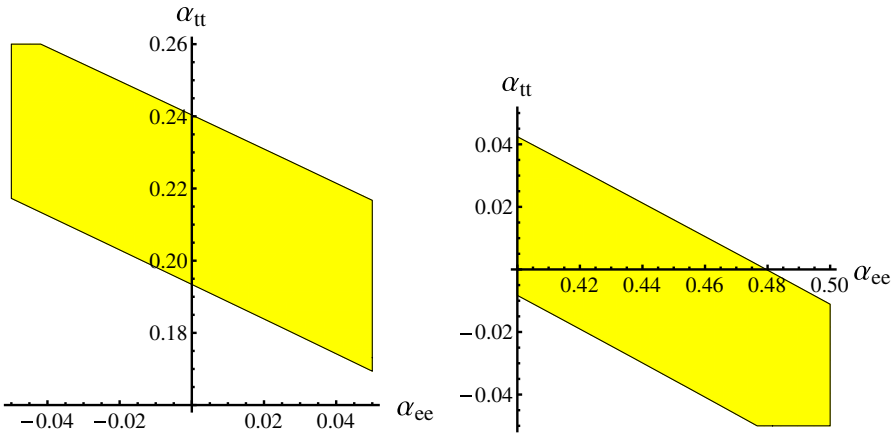

FIG. 11. Constraints in $\alpha_{ee} - \alpha_{tt}$ plane by electron EDM. Fix $m_\eta = 40$ GeV, $|\xi_{tt}| = 0.6$, and $\xi_{ee} = 0.3$.

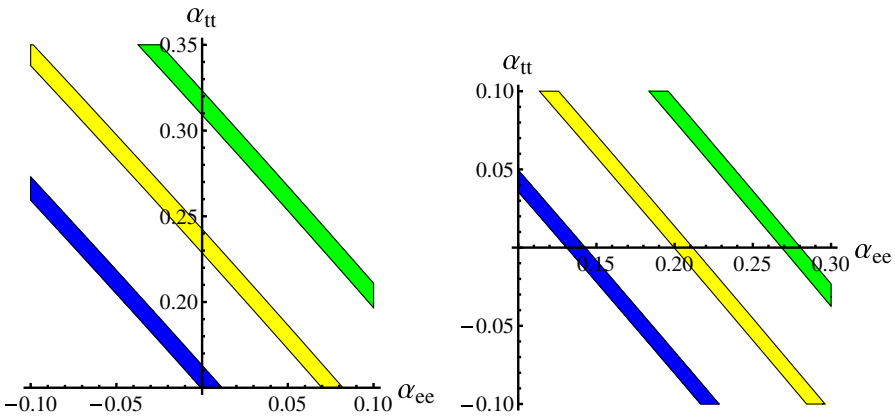

FIG. 12. Constraints in $\alpha_{ee} - \alpha_{tt}$ plane by electron EDM. Fix $m_\eta = 20$ GeV, $|\xi_{tt}| = 0.6$, and $\xi_{ee} = 1$. Yellow regions are allowed for the case without one-loop contribution. Green regions are for one-loop contribution $\Delta d_e = +10^{-27} e \cdot \text{cm}$ while blue regions are for one-loop contribution $\Delta d_e = -10^{-27} e \cdot \text{cm}$.

$$\frac{d_n}{e} \simeq \frac{m_d(\mu_H)}{m_d(\mu_W)}\left(0.63\frac{d_d(\mu_W)}{e} + 0.73\tilde{d}_d(\mu_W)\right) + \frac{m_u(\mu_H)}{m_u(\mu_W)}\left(-0.16\frac{d_u(\mu_W)}{e} + 0.19\tilde{d}_u(\mu_W)\right) + (8.8\ \text{MeV} + 0.17 m_d(\mu_H) + 0.08 m_u(\mu_H))w(\mu_W). \tag{92}$$

Here μ_H is the hadron scale and μ_W is the electroweak scale, $\alpha_s(\mu_W) \approx 0.11$ [108], and $m_d(\mu_H) \approx 4.8$ MeV, $m_u(\mu_H) \approx 2.3$ MeV [29]. $d_q(\mu_W)$, $\tilde{d}_q(\mu_W)$, and $w(\mu_W)$ are all calculated at the electroweak scale.

Numerically, we use the same benchmark points as above. Fixing $|\xi_{uu}| = |\xi_{dd}| = 1$, $|\xi_{tt}| = 0.6$, and $\alpha_{tt} = 0$. For $m_\eta = 20$ and $m_\eta = 40$ GeV, we show the allowed regions in $\alpha_{uu} - \alpha_{dd}$ plane in Fig. 13. There exists cancellation between different contributions as well. From the figures, we can see α_{uu} is almost free, and α_{dd} is constrained in a narrow band. For both cases, $\alpha_{uu} = \alpha_{dd} = 0$ is inside the allowed region, and $\Delta\alpha_{dd} \sim 0.1$. The cancellation behavior is not sensitive to m_η. It is also a strict constraint from neutron EDM, but not so strict as that from electron EDM.

Next, consider the contributions from flavor-changing vertices. Strict constraints from meson mixing (see the text in Sec. III D) require that the contributions for d_n from the $bd\phi$, $sd\phi$, and $uc\phi$ vertices should be less than $\mathcal{O}(10^{-30}) e \cdot \text{cm}$; thus, they are ignorable. But CP violation in the $tu\phi$ vertex would give a larger contribution to d_u and $\tilde{d}_u$ [98,104,105] through the one-loop diagram as the left figure in Fig. 7,

$$\frac{\Delta d_u}{e} = \sum_\phi \frac{m_u |c_{\phi,tu}|^2 \sin(2\alpha_{\phi,tu})}{24\pi^2 v^2} \mathcal{P}_1\left(\frac{m_t^2}{m_\phi^2}\right); \tag{93}$$

$$\Delta\tilde{d}_u = \sum_\phi \frac{m_u |c_{\phi,tu}|^2 \sin(2\alpha_{\phi,tu})}{16\pi^2 v^2} \mathcal{P}_1\left(\frac{m_t^2}{m_\phi^2}\right). \tag{94}$$

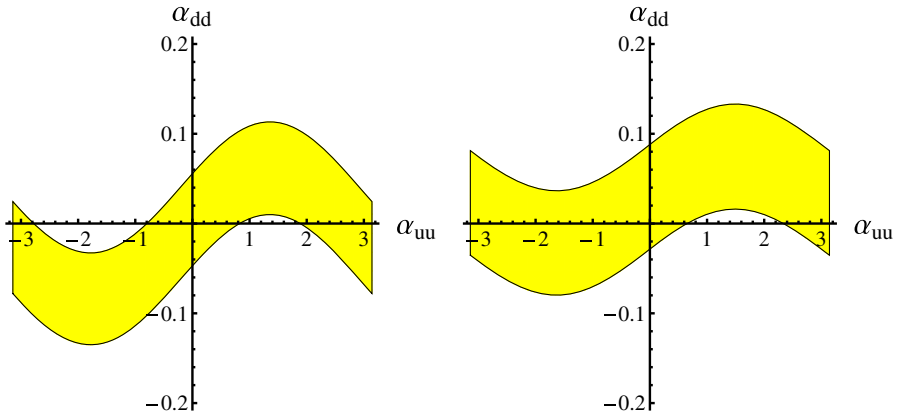

FIG. 13. Allowed region on the $\alpha_{uu} - \alpha_{dd}$ plane with constraint from neutron EDM. We fix $|\xi_{uu}| = |\xi_{uu}| = 1$, $|\xi_{tt}| = 0.6$, and $\alpha_{tt} = 0$. The left figure is for $m_\eta = 20$ GeV and the right one is for $m_\eta = 40$ GeV. All other benchmark points are the same as above. Yellow regions are allowed at 90% C.L.

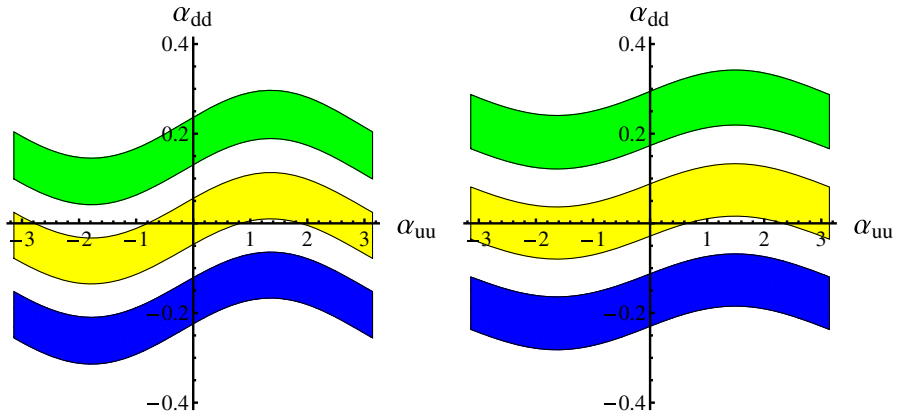

FIG. 14. Allowed region by the constraint from neutron EDM. Benchmark points are the same as above in Fig. 13. Yellow regions are allowed for the case without one-loop contribution. Green regions are for one-loop contribution $\Delta d_n = +10^{-25} e \cdot \text{cm}$ while blue regions are for one-loop contribution $\Delta d_n = -10^{-25} e \cdot \text{cm}$.

The loop function $\mathcal{P}_1(x)$ is listed in (B23) in Sec. B. For $|\xi_{tu}| \sim 1$, the additional contribution to the neutron EDM can reach $\Delta d_n \sim \mathcal{O}(10^{-26} - 10^{-25}) e \cdot \text{cm}$, which would change the cancellation behavior and shift the allowed region a little bit. In Fig. 14, we show the allowed region before and after adding the one-loop contribution $\Delta d_n = \pm 10^{-25} e \cdot \text{cm}$. The case $|\Delta d_n| \gtrsim 6 \times 10^{-25} e \cdot \text{cm}$ is excluded for this benchmark points choice because enough cancellation between different contributions cannot be generated.

TABLE IV. Recent experimental and theoretical results for $B^0_{(s)} \to \mu^+\mu^-$ decay branching ratios.

Result	$\text{Br}(B^0_s \to \mu^+\mu^-)$	$\text{Br}(B^0 \to \mu^+\mu^-)$
CMS	$(2.8^{+1.1}_{-0.9}) \times 10^{-9}$	$(4.4^{+2.2}_{-1.9}) \times 10^{-10}$
LHCb	$(2.7^{+1.1}_{-0.9}) \times 10^{-9}$	$(3.3^{+2.4}_{-2.1}) \times 10^{-10}$
Combined	$(2.8^{+0.7}_{-0.6}) \times 10^{-9}$	$(3.9^{+1.6}_{-1.4}) \times 10^{-10}$
SM prediction	$(3.65 \pm 0.23) \times 10^{-9}$	$(1.06 \pm 0.09) \times 10^{-10}$

H. Constraints from B-meson rare decays

The leptonic decay $B^0_{(s)} \to \mu^+\mu^-$ was measured by CMS and LHCb collaborations and the results [109–111] are listed in Table IV together with their SM predictions [112,113]. Both measurements are almost consistent with SM predictions[17]; thus, new physics contributions would be limited.

The tree-level contributions to $B^0_{(s)} \to \mu^+\mu^-$ are negligible [1] due to the constraints from B-meson mixing. Here we consider the charged Higgs contribution only. In this scenario, $m_\pm \sim v$ is favored as above. For

[17]The CMS result for $\text{Br}(B^0 \to \mu^+\mu^-)$ has a deviation from SM prediction at about 2σ level. The same thing happens to the combined result for $\text{Br}(B^0 \to \mu^+\mu^-)$.

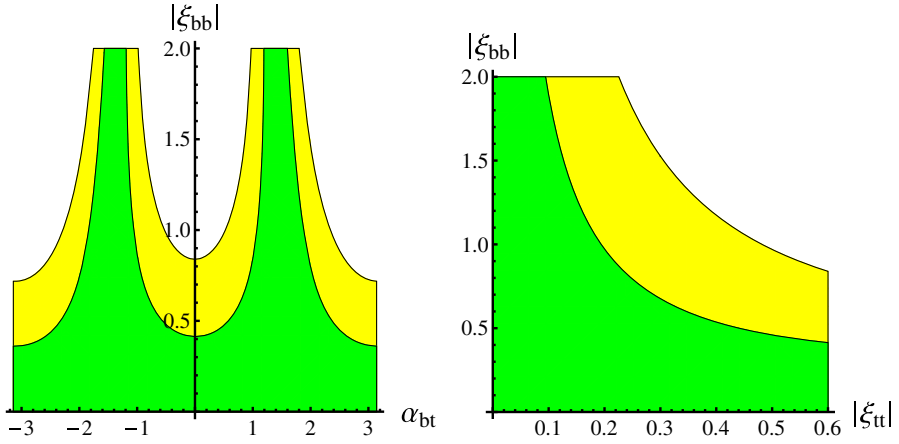

FIG. 15. Constraints by $\mathrm{Br}(\bar{B} \to X_s\gamma)$ fixing $m_\pm = 200$ GeV. In the left figure, we take $|\xi_{tt}| = 0.6$ and plot the allowed region in $|\xi_{bb}| - \alpha_{bt}$ plane. In the right figure, we take $\alpha_{bt} = 0$ and plot the allowed region in $|\xi_{bb}| - |\xi_{tt}|$ plane. In both figures, green regions are allowed at 68% C.L. and the yellow regions are allowed at 95% C.L.

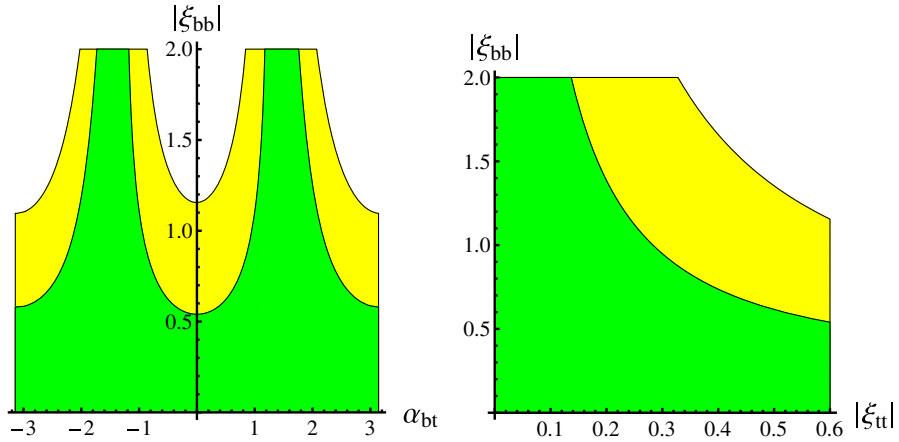

FIG. 16. Constraints by $\mathrm{Br}(\bar{B} \to X_s\gamma)$ fixing $m_\pm = 300$ GeV. All other sets are the same as those in Figure 15.

$|\xi_{bb,dd,\ell\ell}| \sim \mathcal{O}(1)$, the modified branching ratio for $B^0_{(s)} \to \mu^+\mu^-$ should be [114]

$$\frac{\mathrm{Br}(B^0_{(s)} \to \mu^+\mu^-)}{\mathrm{Br}_{\mathrm{SM}}(B^0_{(s)} \to \mu^+\mu^-)} = \left(1 - \frac{|\xi_{tt}|^2}{\eta}\frac{\mathcal{Y}_{\mathrm{2HDM}}(m_t^2/m_W^2, m_\pm^2/m_W^2)}{\mathcal{Y}_{\mathrm{SM}}(m_t^2/m_W^2)}\right)^2 \quad (95)$$

where $\eta = 0.987$ is the QCD and electroweak correlation factor and the loop functions $\mathcal{Y}_i$ are listed in (B25)–(B26) in Sec. B. Numerically, consider $B^0_s \to \mu^+\mu^-$, both CMS and LHCb results give

$$|\xi_{tt}| \lesssim (0.7\text{–}0.8) \quad (96)$$

at 95% C.L. which is near the constraint by B meson mixing in (58). For $B^0_d \to \mu^+\mu^-$ decay, these regions are also allowed at 95% C.L. by both CMS and LHCb results.[18]

The world averaged value for B radiative decay branching ratio reads $\mathrm{Br}_{\mathrm{ave}}(\bar{B} \to X_s\gamma) = (3.43 \pm 0.22) \times 10^{-4}$ [67] which is consistent with its SM prediction $\mathrm{Br}_{\mathrm{SM}}(\bar{B} \to X_s\gamma) = (3.36 \pm 0.23) \times 10^{-4}$ [115]. In 2HDM, according to (25), a charged Higgs boson can also run in the loop instead of $W^\pm$ for the radiative decay process; thus, the branching ratio can be modified. In type II 2HDM, the charged Higgs mass is constrained to be larger than about 410 GeV [116][19] at 95% C.L. But in a general 2HDM, a lighter charged Higgs boson may be allowed [1]. Different

[18]If considering the combined result, $|\xi_{tt}| \lesssim (0.5\text{–}0.6)$ is still allowed by data due to $B^0_s \to \mu^+\mu^-$ which is a bit stricter than that in (58). For $B^0_d \to \mu^+\mu^-$, we also need $|\xi_{tt}| \gtrsim (0.2\text{–}0.3)$ at 95% C.L. because the combined deviation between $\mathrm{Br}(B^0 \to \mu^+\mu^-)$ and its SM prediction is a bit larger than 2σ.

[19]This value is different from the data in the text of [116] because the SM prediction result was updated in [115] recently.

from leptonic decay, the radiative decay branching ratio is sensitive to not only $m_\pm$ and ξ_{tt}, but also ξ_{bb}. For a general case, $\alpha_{bt} \equiv \arg(\xi_{bb}/\xi_{tt})$ is also a free parameter. Based on [116] and the mathematica code, we plot the constraints on these parameters in Figs. 15 and 16, fixing $m_\pm = 200$ and $m_\pm = 300$ GeV, respectively. From the figures, we can see that for $|\xi_{tt}| = 0.6$, for most α_{bt} choices, we have $|\xi_{bb}| \lesssim 1$; however, for some α_{bt} choices, a larger $|\xi_{bb}|$ is also allowed. While for fixed α_{bt}, there is also a larger allowed region in $|\xi_{bb}| - |\xi_{tt}|$ plane. The constraint is not so strict as that for the type II 2HDM because more parameters are free, just like the case in [1].

IV. PREDICTIONS AND FUTURE TESTS FOR THIS SCENARIO

We have discussed all the constraints on the Lee model in an alternative scenario which is weakly coupled. As shown above, it is still not excluded by experimental results. Comparing with the scenario in [1], the particle spectrum are the same. But in this scenario, all the scalars are required to have their mass around electroweak scale or lighter. Especially, the lightest scalar is required to have its mass $m_\eta \sim \mathcal{O}(10\ \text{GeV})$ which means new physics is hidden in the scale lower than electroweak scale. That's different from the scenario in [1] in which new physics would appear at $\mathcal{O}(\text{TeV})$ or higher scale.

In this scenario, the couplings of the 125 GeV Higgs boson is SM-like, but other particles are not decoupled; thus, they would face future tests at colliders. A lighter scalar can also appear through the Higgs decay channels $h \to Z\eta$, $\eta\eta$, which are worth searching. Different scalars may also be produced associated with each other or with the heavy quark (pair). $h \to Z\eta$, $\eta\eta$ rare decays would also be constrained by Higgs signal strengths which would be measured precisely in the future. Experiments on flavor-changing processes and EDM measurements would also help to confirm or exclude this scenario indirectly.

A. Direct searches for extra scalars at future colliders

The key prediction of this scenario (the weakly coupled Lee model) is a light particle η with a mass of $\mathcal{O}(10\ \text{GeV})$. It should be a CP-mixing state with the pseudoscalar component dominant. Its low mass is correlated with the smallness of the CP violation. At the LHC, it certainly can be produced through gluon fusion or $b\bar{b}$ fusion with a large cross section, but such a light particle would be hidden below the huge QCD background [13]; thus, it is difficult to discover. At the LHC, with $\sqrt{s} = (13\text{–}14)$ TeV, η can also be produced in associated with top quark pair with a cross section of $\mathcal{O}(0.1)$ pb [117]. According to [117], at the LHC with $\sqrt{s} = 14$ TeV and 3 ab^{-1} luminosity, for $m_\eta \sim$ (20–40) GeV, the constraint $|\xi_{tt}| \lesssim (0.34\text{–}0.54)$ at 95% C.L. would be achieved assuming no positive results. It would be stricter than all the recent constraints obtained from indirect processes. On the other hand, for $m_\eta \sim (30\text{–}40)$ GeV, the benchmark case $|\xi_{tt}| = 0.6$ would be discovered at more than 5σ.

η can also appear as the decay final state of other scalars, such as h, $H \to \eta\eta$, $Z\eta$, etc. We will study the cascade decay channels in detail in the future. LHeC [118,119] would be a better collider in searching for the exotic Higgs decays [120]. At future e^+e^- colliders [121–124], it is also possible to discover η through Higgs rare decay processes, such as $e^+e^- \to Zh(\to \eta\eta)$. At the Higgs factories with $\sqrt{s} \sim (240\text{–}250)$ GeV like CEPC [123] or TLEP [121], this process can be discovered at 5σ with 5 ab^{-1} luminosity if $\text{Br}(h \to \eta\eta) > 10^{-3}$ [123]. η can also be produced in associated with Z or h at CEPC or TLEP. With a roughly estimation comparing with LEP results [50–52,65] we used in Sec. III A, using $\mathcal{O}(10^2\text{–}10^3)$ fb^{-1} luminosity, the sensitivity to $c_{\eta,V}$ and $c_{h\eta}(= c_{H,V})$ would improve at least an order. At e^+e^- colliders with $\sqrt{s} > m_\eta + m_H$, it is possible to produce η and H through $e^+e^- \to \eta H$.[20] It's worth noting that under weak-coupling assumption, m_H should be around the electroweak scale, and $c_{\eta H} = c_h \sim 1$ would never be suppressed; thus, this is also a key process to confirm or exclude this scenario at future e^+e^- colliders.

For the heavy Higgs boson H, a mass around v is required; thus it is possible to discover it at the LHC [125]. For $m_H \sim (200\text{–}300)$ GeV, we choose $|\xi_{tt}| = 0.6$ and $c_{H,V} = 0.3$ from above, with the cross section $\sigma(pp \to H \to ZZ) \sim (120\text{–}200)$ fb according to [126] at the future LHC with $\sqrt{s} = 14$ TeV. It is larger than the 5σ discovery threshold (50–100) fb using 3 ab^{-1} luminosity [125]; thus, it could be easily discovered. If no signal evidence were found, according to [125], the 95% C.L. limit for $\sigma(pp \to H \to ZZ)$ would be (20–40) fb for the mass region $m_H \sim (200\text{–}300)$ GeV. Since the dominant production channel for H is gluon fusion, this result means the future LHC would be able to set the constraint

$$|\xi_{tt}| c_{H,V} \lesssim 0.08 \tag{97}$$

at 95% C.L. if no evidence for this channel were found.

Through the oblique parameter constraints, the charged Higgs mass is around v in this scenario. It must face the direct searches at the LHC or e^+e^- colliders. At the LHC, it can be produced through $gb \to tH^-$ associated production [127] which was used to search for the charged Higgs boson in [57]. For a light charged Higgs with $m_\pm \sim (200\text{–}300)$ GeV, for $|\xi_{tt}| \sim 0.6$ and $|\xi_{bb}| \sim \mathcal{O}(1)$, it would be discovered at the LHC with $\sqrt{s} = (13\text{–}14)$ TeV and 300 fb^{-1} luminosity, and the polarization of the top quark would also be useful to test the chiral structure in the tbH^- vertex [128–130]. At the e^+e^- colliders with

[20] If $m_H \sim 200$ GeV, the Higgs factory mentioned above is also allowed for this process.

TABLE V. Examples for main processes which would be useful to test this scenario at future pp collider. "*" means we will study this process in detail in the future. In this table, all masses are chosen as: $m_\eta = 40$ $m_h = 125$, and $m_H = m_\pm = 300$ GeV as an example. The benchmark points listed here for collider or model parameters are possible choices but not the only choice for the corresponding processes.

Collider	Process	$\sqrt{s}$ (TeV)	Couplings and/or branching ratios	Cross section (pb)	Implications
LHC	$pp \to t\bar{t}\eta$	14	$\lvert\xi_{tt}\rvert = 0.6$	0.18	Over 5σ discovery with 3 ab^{-1} luminosity assuming $\mathrm{Br}_{\eta\to b\bar{b}} = 1$.
LHC	$pp \to H(ZZ)$	14	$\lvert\xi_{tt}\rvert = 0.6$, $\mathrm{Br}_{H\to ZZ} = 3\%$	0.12	Over 5σ discovery with 3 ab^{-1} luminosity.
LHC	$pp \to H(Z\eta, \eta\eta)$	14	$c_{H\eta} = c_{h,V} = 0.95$, $\lvert\xi_{tt}\rvert = 0.6$, $g_{H\eta\eta} \sim 1$	$4 \times \mathrm{Br}_{H\to Z\eta,\eta\eta}$	*To be studied.
LHC	$pp(bg) \to tH^-(\bar{t}b)$	14	$\lvert\xi_{tt}\rvert = 0.6$, $\lvert\xi_{bb}\rvert \lesssim 1$, $\mathrm{Br}_{H^-\to\bar{t}b} = 1$	0.6	5σ discovery with $\mathcal{O}(10^2)$ fb^{-1} luminosity.

TABLE VI. Examples for main processes which would be useful to test this scenario at future e^+e^- colliders. "*" means we will study this process in detail in the future. In this table, all masses are chosen as: $m_\eta = 40$, $m_h = 125$ and $m_H = m_\pm = 300$ GeV as an example. The benchmark points listed here for collider or model parameters are possible choices but not the only choice for the corresponding processes.

Collider	Process	$\sqrt{s}$ (TeV)	Couplings and/or branching ratios	Cross section (pb)	Implications
CEPC	$e^+e^- \to Z\eta$	0.25	$c_{\eta,V} = 0.1$	4.4×10^{-3}	*Sensitivity to $c_{\eta,V}$ would reach $\mathcal{O}(10^{-2})$ with 5 ab^{-1} luminosity.
CEPC	$e^+e^- \to h\eta$	0.25	$c_{h\eta} = c_{H,V} = 0.3$	7.3×10^{-3}	*Sensitivity to $c_{H,V}$ would reach $\mathcal{O}(10^{-2})$ with 5 ab^{-1} luminosity.
CEPC	$e^+e^- \to Zh(\eta\eta)$	0.25	$c_{h,V} = 0.95$, $\mathrm{Br}_{\eta\to b\bar{b}} = 1$	$0.19 \times \mathrm{Br}_{h\to\eta\eta}$	5σ discovery with 5 ab^{-1} luminosity if $\mathrm{Br}_{h\to\eta\eta} > 10^{-3}$
ILC	$e^+e^- \to H\eta$	0.5	$c_{h,V} = 0.95$	1×10^{-2}	*To be studied.
ILC	$e^+e^- \to H^+H^-$	0.8	$\mathrm{Br}_{H^-\to\bar{t}b} = 1$	1.4×10^{-2}	Cross section can be measured to 9% with 1 ab^{-1} luminosity.

$\sqrt{s} \gtrsim 500$ GeV, we can discover the charged Higgs boson through the $e^+e^- \to H^+H^-$ process [131,132]. This process would not be suppressed; thus, it is useful to confirm or exclude this scenario. In Tables V and VI, we summarize the mentioned channel above which would be useful for testing this scenario in the future [117,123,125–133].

If all three neutral scalars and their couplings to VV were discovered in the future, the associated productions for any two scalars would be important to confirm CP violation in the Higgs sector as well. Since in a general model, if no CP violation exists in the scalar sector, all three discovered neutral scalars should be CP even[21]; thus, there would be no direct h_ih_jZ vertices. The $e^+e^- \to h_ih_j$ process would be loop induced in this case; thus, the cross section would be highly suppressed. If the cross sections show that there exists tree-level h_ih_jZ vertices,[22] the scalars must contain different CP components and, thus, we would be able to confirm CP violation in the scalar sector [133].[23]

B. Future measurements on the 125 GeV Higgs boson

In this scenario, the couplings between the 125 GeV Higgs boson h and SM particles should be SM-like. Exotic decay channels $h \to \eta\eta$ or $Z\eta$ make the total width of h larger, which would also affect other decay channels of h. In the future, the LHC will be able to measure the signal strengths $h \to \gamma\gamma$, ZZ^*, WW^*, $b\bar{b}$, $\tau^+\tau^-$ to the precision (11–14)% with 300 fb^{-1} luminosity, and (7–8)% with 3 ab^{-1} luminosity [134,135].

In this scenario, the modification of Higgs couplings to fermions or gauge bosons should be at percent level, for some cases it can reach 10%. Under this assumption, if the future signal strengths were all consistent with SM prediction, we perform a global-fit and estimate that at least

[21]This case cannot appear in 2HDM because there must be additional scalar degree of freedoms, such as another Higgs doublet.

[22]For example, if the cross sections satisfied the relations in (A15).

[23]Notice this is a model-independent method to confirm CP-violation in scalar sector. But it cannot be used to exclude CP-violation in the scalar sector because, in some models, there are no direct h_ih_jZ vertices even if CP violation exists in the scalar sector.

$\Gamma_{\rm exo} \lesssim (0.4\text{–}0.6)$ MeV (or equivalently $\mathrm{Br}_{\rm exo} \lesssim (10\text{–}15)\%$) would still be allowed in this scenario. The direct measurements at the future LHC cannot reach the sensitivity to test the modification of Higgs signal strengths from those in SM.

At future e^+e^- colliders, such as the Higgs factories CEPC [123] or ILC [124,131] with $\sqrt{s} \sim (240\text{–}250)$ GeV, to the luminosity of $\mathcal{O}(\mathrm{ab}^{-1})$, all the channels mentioned above together with the Higgs total width can be measured to percent level or even better. For $c_{h,V} \sim 0.95$, $\Delta\sigma_{Zh}/\sigma_{Zh} \sim 10\%$ which can be measured with $\mathcal{O}(0.1\ \mathrm{ab}^{-1})$ luminosity. The precision measurements on $h \to b\bar{b}$, $\tau^+\tau^-$ are also helpful to distinguish this scenario from SM. If no deviations were found, $|\xi_{bb,\tau\tau}|$ would be constrained to $\mathcal{O}(1)$. For $h \to gg$ decay, it is sensitive to both $|c_{h,t}|$ and $\alpha_{h,t}$. The exotic decays $h \to \eta\eta$, $Z\eta$ would also be discovered or further constrained at the Higgs factory.

CP violation is a main component of the Lee model, for example, the $hf\bar{f}$ couplings would contain *CP* violation. For the τ lepton and top quark, the decay distribution would include its polarization information; thus, it is possible to test the *CP*-violation effects in the $ht\bar{t}$ and $h\tau^+\tau^-$ vertices [131]. At the LHC with $\sqrt{s} =$ 13 TeV and $3\mathrm{ab}^{-1}$ luminosity, using the $h \to \tau^+\tau^-$ decay mode, it is possible to measure $\alpha_{h,\tau}$ to the sensitivity $\Delta\alpha_{h,\tau} \sim 4°$ with the help of the final states distribution in the τ decay [136], while at the e^+e^- collider, with $\sqrt{s} =$ 250 GeV and 1 ab^{-1} luminosity, this sensitivity would reach $\Delta\alpha_{h,\tau} \sim 2.8°$ [137], both of which are enough to test this scenario. For the $ht\bar{t}$ coupling, we can use $e^+e^- \to t\bar{t}h$ associated production to test $\alpha_{h,t}$ [105,131,138], with $\sqrt{s} > 2m_t + m_h \sim 470$ GeV.

C. EDM for third-generation fermions

As mentioned above, the polarization of a τ lepton or top quark can affect on the distribution of its decay final states. With this property, it may be possible to test their anomalous electroweak couplings including EDM. For a heavy fermion such as τ, b, t, if one-loop contribution to *CP* violation (see Figure 7) exists, the Barr-Zee-type contribution would be ignorable. The one-loop contribution reads [104,105]

$$d_f = \frac{Q_f m_f^3}{16\pi^2 v^2} \sum_\phi \frac{|c_{\phi,f}|^2 \sin(2\alpha_{\phi,f})}{m_\phi^2} \mathcal{P}_2\left(\frac{m_f^2}{m_\phi^2}\right), \quad (98)$$

where the loop function $\mathcal{P}_2(x)$ is listed in (B24) in Sec. B.

For a τ lepton,

$$|d_\tau| \lesssim \frac{m_\tau^3 |\xi_{\tau\tau}|^2}{16\pi^2 v^2 m_\eta^2} \left(\ln\left(\frac{m_\eta^2}{m_\tau^2}\right) - \frac{3}{2}\right) \sim 10^{-22} |\xi_{\tau\tau}|^2 e \cdot \mathrm{cm}. \quad (99)$$

If $|\xi_{\tau\tau}| \sim 1$, it is still far away from the future sensitivity of τ EDM, around $\mathcal{O}(10^{-19} e \cdot \mathrm{cm})$, given by SuperB [139,140] with $\sqrt{s} = m_{\Upsilon(4S)}$ and (50–75) ab^{-1} luminosity or CEPC [123] with $\sqrt{s} = 240$ GeV and 5 ab^{-1} luminosity. But for a top quark, it can be larger due to its large mass. With the benchmark points in Table I, for $|\xi_{tt}| = 0.6$ and $m_\eta \sim (20\text{–}40)$ GeV, $|d_t|$ can reach $\mathcal{O}(10^{-19}\text{–}10^{-18}) e \cdot \mathrm{cm}$ which would be possibly tested at future e^+e^- colliders with $\mathcal{O}(\mathrm{ab}^{-1})$ luminosity [105,141].

D. Future tests in flavor physics

At the future SuperB with (50–75) ab^{-1} luminosity [139,140] and the LHCb with 50 fb^{-1} luminosity [142] experiments, for $B^0_{(s)} - \bar{B}^0_{(s)}$ mixing, the sensitivity to $\Delta_{B(B_s)}$ in (52) would reach $(3\text{–}7) \times 10^{-2}$ given by [74]. With these sensitivities, if no deviations in B meson mixing were found, it would require $|\xi_{tt}| \lesssim (0.2\text{–}0.3)$ at 95% C.L., while the benchmark point we choose in the text above, $|\xi_{tt}| \sim 0.6$, would lead to at least a 5σ deviation from the SM prediction in B meson mixing results.

Another important indirect constraint on ξ_{tt} comes from the leptonic decay of B meson. Future measurements on $\mathrm{Br}(B^0_s \to \mu^+\mu^-)$ would reach 12% with 3 ab^{-1} luminosity by CMS [143] and 4% with 50 fb^{-1} by LHCb [142]. If no deviation from SM were found, it would require $|\xi_{tt}| \lesssim 0.4$ at 95% C.L. If $|\xi_{tt}| = 0.6$, the LHCb result would be larger than the SM prediction at 3σ level.

At the LHC with $\sqrt{s} = 13$ TeV and 300 fb^{-1} luminosity, if no LFV signal were found, it would require $\mathrm{Br}(h \to \mu^\pm\tau^\mp) < 7.7 \times 10^{-4}$ at 95% C.L. [144], or equivalently $|\xi_{\mu\tau}| \lesssim (1.1\text{–}3.5)$ which is still not strict. To 3 ab^{-1}, the upper limit for $|\xi_{\mu\tau}|$ would reduce to (0.6–2.0). At the SuperB factory with 75 ab^{-1} luminosity, $\mathrm{Br}(\tau \to \mu\gamma)$ can be constrained to less than 2.4×10^{-9} at 90% C.L., or be discovered at 3σ level if it is larger than 5.4×10^{-9} [140].

According to (76) and (78) taking the benchmark points in Table I, fix $|\xi_{\mu\tau}| = |\xi_{\tau\mu}| = |\xi_{\tau\tau}| = 1$ and $\xi_{tt} = 0.6$, we plot the $\mathrm{Br}(\tau \to \mu\gamma)$ distributions in $\alpha_{tt} - \alpha_{\tau\tau}$ plane in Figure 17, for $m_\eta = 20$ (left) and $m_\eta = 40$ GeV (right). If no evidence for $\tau \to \mu\gamma$ were found, the parameters would be constrained to be in the green regions, while if the parameters were in blue (orange) regions, $\tau \to \mu\gamma$ would be discovered at the $3(5)\sigma$ level at the SuperB factory with $75\mathrm{ab}^{-1}$ luminosity. Fixing $|\xi_{\mu\tau}| = |\xi_{\tau\mu}| = 1$ and leaving other parameters free, if no evidence were found at SuperB, $|\xi_{\tau\tau}|$ would be required less than 1.2 for the $m_\eta = 20$ GeV case or less than 2.6 for the $m_\eta = 40$ GeV case.

At the SuperB factory, the dominant background for $\tau \to \mu\gamma$ should be $e^+e^- \to \tau^+\tau^-\gamma$ [139] which would be suppressed at a collider with $\sqrt{s}$ not far above $2m_\tau$, such as Super tau-charm factory [145]. At Super tau-charm factory with 10 ab^{-1} luminosity, the sensitivity of $\mathrm{Br}(\tau \to \mu\gamma)$ would reach around 2×10^{-10} [146], which can give

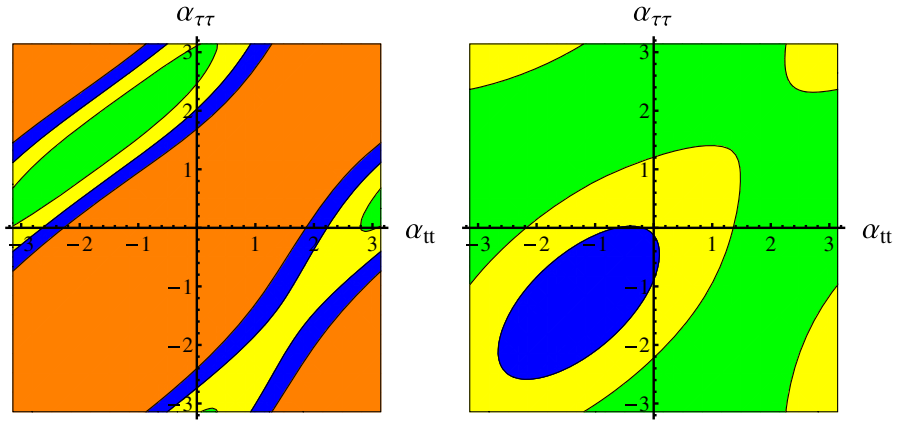

FIG. 17. Distributions of $\mathrm{Br}(\tau \to \mu\gamma)$ in $\alpha_{tt} - \alpha_{\tau\tau}$ plane with the benchmark points in Sec. III F. The left figure is for $m_\eta = 20$ GeV and the right figure is for $m_\eta = 40$ GeV. In both figures, $|\xi_{\mu\tau}| = |\xi_{\tau\mu}| = |\xi_{\tau\tau}| = 1$ and $\xi_{tt} = 0.6$. The green regions are for $\mathrm{Br}(\tau \to \mu\gamma) \leq 2.4 \times 10^{-9}$; the yellow regions are for $2.4 \times 10^{-9} < \mathrm{Br}(\tau \to \mu\gamma) \leq 5.4 \times 10^{-9}$; the blue regions are for $5.4 \times 10^{-9} < \mathrm{Br}(\tau \to \mu\gamma) \leq 9 \times 10^{-9}$; and the orange regions are for $\mathrm{Br}(\tau \to \mu\gamma) > 9 \times 10^{-9}$.

further constraints. Future MEG experiments on $\mathrm{Br}(\mu \to e\gamma)$ would reach the sensitivity 6×10^{-14} in three years [147], which can give stricter constraints for all the three LFV couplings $\xi_{e\mu,e\tau,\mu\tau}$.

V. CONCLUSIONS AND DISCUSSIONS

In this paper, based on weakly coupled spontaneous CP-violation 2HDM (named Lee model), using the correlation between the lightest scalar and smallness of CP violation through small $t_\beta s_\xi$ which was proposed in our recent paper [1], we predicted that a light CP-mixing scalar with its mass of $\mathcal{O}(10\ \mathrm{GeV})$ should exist. It is pseudoscalar dominant with only about $\mathcal{O}(0.1)$ scalar component. In this scenario, other scalars' masses are all around the electroweak scale v. It's attractive because there should be new physics hidden at $\mathcal{O}(10\ \mathrm{GeV})$ scale which is below the electroweak scale, different from the scenario we discussed in [1] in which the Higgs sector is strong-coupled and new physics appear at $\mathcal{O}(\mathrm{TeV})$ or higher scale.

We discussed all experimental constraints, at both high and low energy, for two typical lightest scalar (η) masses, $m_\eta = 20$ GeV ($h \to Z\eta$ decay allowed) and $m_\eta = 40$ GeV ($h \to Z\eta$ decay forbidden). For these η masses, $c_{\eta,V} \sim 0.1$ is required theoretically and it is also allowed by data. The 125 GeV Higgs boson h has SM-like couplings to fermions and gauge bosons. With a global fit to Higgs signal strengths, branching ratio for exotic decay channels are constrained to less than about 30%, which leads to strict constraints on $h\eta\eta$ (and $hZ\eta$ if $m_\eta < 34$ GeV) couplings. The constraints from oblique parameters require $m_\pm \sim m_H \sim v$ under the weak-coupling assumption. The typical benchmark points listed in Table I are chosen according to these constraints.

In the Lee model, there is no additional discrete symmetry except CP; thus, there may exist flavor-changing interactions at the tree level. We adopted the Cheng-Sher ansatz to parametrize the flavor-changing effects. High energy processes including top flavor-changing interactions cannot give strict constraints. The most strict constraint from high energy experiments comes from an indirect test, top quark widths limit from $t\bar{t}$ pair production, which requires $|\xi_{tc}| \lesssim 1$. A more strict constraint comes from $D^0 - \bar{D}^0$ mixing which requires $|\xi_{tc}\xi_{tu}| \lesssim 6$. All other $|\xi_{ij}|$ in quark sector are constrained to be less than around $\mathcal{O}(10^{-2})$, through meson mixing measurements. In the lepton sector, indirect tests (especially radiative LFV decays) require $|\xi_{\mu\tau}| \lesssim \mathcal{O}(1)$, while the upper limits on $|\xi_{e\mu}|$ or $|\xi_{e\tau}\xi_{\mu\tau}|$ are of $\mathcal{O}(10^{-2})$. EDM tests also favor $|\xi_{e\tau,ut}| \lesssim \mathcal{O}(1)$. These constraints are usually stricter than those in [1] as we discussed, that's because in this scenario, a lighter scalar would give more significant contribution to the flavor-changing processes.

B meson mixing and B leptonic decay processes are all sensitive to ξ_{tt}. With these data, $|\xi_{tt}| \lesssim 0.6$ is favored at 95% C.L., which is the reason why in most parts of the text we choose $|\xi_{tt}| = 0.6$ as a benchmark point. The B radiative decay process is sensitive to both ξ_{tt} and ξ_{bb}. With the assumption $m_\pm \sim (200\text{–}300)$ GeV and $|\xi_{tt}| = 0.6$, $\xi_{bb} \lesssim \mathcal{O}(1)$ is allowed by data. That is a difference between this scenario and type II 2HDM in which the charged Higgs should be heavier than around 410 GeV at 95% C.L.

The EDM constraints are also strict just like the scenario we discussed in [1]. For both the electron and neutron EDM, we need a large cancellation between different contributions, as shown in Fig. 8–Fig. 14. In each of the figures, the two shown parameters are constrained in a narrow band which means a strong correlation between them.

We also discussed the future tests for this scenario. For the lightest scalar η, the dominant ways to discover it at the LHC are associated production $pp \to t\bar{t}\eta$ and cascade

decay $pp \to h$, $H \to \eta\eta$, $Z\eta$. However, since the heaviest neutral scalar is also required to have its mass around v, it can also be searched through $Z\eta$ or VV final states. At the LHeC or e^+e^- colliders, the exotic decays $h \to \eta\eta$, $Z\eta$ would be tested. In particular, at the Higgs factory, with $\mathcal{O}(10\text{–}10^2)$ fb^{-1} luminosity, $c_{\eta,V} \sim 0.1$ can be discovered at $(3\text{–}5)\sigma$ through rescaling the LEP constraints. If nothing were found, constraints on $c_{\eta,V}$ would improve an order which also implies $m_\eta \sim \mathcal{O}(\text{GeV})$; thus, this scenario is disfavored. The mass of the charged Higgs boson is predicted to be around v which is in the range to be discovered at the future LHC or e^+e^- colliders with $\sqrt{s} \gtrsim 500$ GeV, using $\mathcal{O}(0.1\text{–}1)$ ab^{-1} luminosity. Note that the $e^+e^- \to H^+H^-$ process cannot be suppressed with fixed $m_\pm$. If nothing were found, this scenario would be excluded.

If all three scalars are discovered and they all have direct vertices to massive gauge boson pairs, the Z-mediated Higgs associated pair production via $e^+e^- \to h_i h_j$ would be a key observable to confirm CP violation in the scalar sector. It can be used to distinguish Lee model and models in which the scalar sector contains more CP-even degrees of freedom but no CP violation.

Indirect tests on B meson mixing and B leptonic decay can be used to test a nonzero ξ_{tt} or give a stricter limit on $|\xi_{tt}|$. For the case $|\xi_{tt}| = 0.6$ we used in this paper, there would appear $(3\text{–}5)\sigma$ deviations in these experiments. If nothing anomalous were found, $|\xi_{tt}|$ would be pushed to less than about (0.2–0.3). Radiative LFV decays would also confirm a nonzero LFV vertex or push them to a smaller number, depending on the results positive or negative.

In this attractive scenario, all new physics would appear below or at electroweak scale which behaves different from most models in which new physics appear at or above $\mathcal{O}(\text{TeV})$ scale. It means this scenario is testable. The roughly estimation showed it is able to discover or exclude this scenario, especially for η who is hidden at $\mathcal{O}(10\text{ GeV})$ scale. It is also possible to distinguish whether CP violation in the Higgs sector exists if all neutral scalars were found. Thus, it is worth further detailed study, especially at future e^+e^- colliders.

ACKNOWLEDGMENTS

We thank Chen Zhang for helpful discussions. This work was supported in part by the Natural Science Foundation of China (Grants No. 11135003 and No. 11375014).

APPENDIX A: SPECTRUM AND COUPLINGS

The expansion for the neutral scalar mass matrix

$$\begin{pmatrix} (\lambda_4-\lambda_7)s_\xi^2 & -((\lambda_4-\lambda_7)s_\beta c_\xi + \lambda_2 c_\beta)s_\xi & -((\lambda_4-\lambda_7)c_\beta c_\xi + \lambda_5 s_\beta)s_\xi \\ & 4\lambda_1 c_\beta^2 + \lambda_2 s_{2\beta} c_\xi + (\lambda_4-\lambda_7)s_\beta^2 c_\xi^2 & ((\lambda_3+\lambda_7)+(\lambda_4-\lambda_7)c_\xi^2/2)s_{2\beta} \\ & & +\lambda_2 c_\beta^2 c_\xi + \lambda_5 s_\beta^2 c_\xi \\ & & (\lambda_4-\lambda_7)c_\beta^2 c_\xi^2 \\ & & +\lambda_5 s_{2\beta} c_\xi + 4\lambda_6 s_\beta^2 \end{pmatrix} \tag{A1}$$

is $\tilde{m} = \tilde{m}_0 + (t_\beta s_\xi)\tilde{m}_1 + (t_\beta s_\xi)^2 \tilde{m}_2 + \ldots$. To the first order, we have

$$m_\eta = 0, \qquad m_{h,H} = \frac{v}{2}\sqrt{(4\lambda_1+\lambda_4-\lambda_7) \mp ((4\lambda_1-(\lambda_4-\lambda_7))c_{2\theta} + 2\lambda_2 s_{2\theta})}, \tag{A2}$$

where $\theta = (1/2)\arctan(2\lambda_2/(4\lambda_1-\lambda_4+\lambda_7))$ is the mixing angle. The scalar fields are

$$\eta_0 = I_2, \qquad \begin{pmatrix} h \\ H \end{pmatrix}_0 = \begin{pmatrix} c_\theta & s_\theta \\ -s_\theta & c_\theta \end{pmatrix}\begin{pmatrix} R_1 \\ R_2 \end{pmatrix}. \tag{A3}$$

Calculation by the perturbation method to the leading order of $(t_\beta s_\xi)$ gives

$$\eta = I_2 - (t_\beta s_\xi)\left(\frac{(\tilde{m}_1)_{12}}{(\tilde{m}_0)_{22}}(c_\theta R_1 + s_\theta R_2) + \frac{(\tilde{m}_1)_{13}}{(\tilde{m}_0)_{33}}(c_\theta R_2 - s_\theta R_1)\right) - t_\beta c_\xi I_1; \tag{A4}$$

$$h = c_{\theta'} R_1 + s_{\theta'} R_2 + \frac{(\tilde{m}_1)_{12}}{(\tilde{m}_0)_{22}} (t_\beta s_\xi) I_2; \tag{A5}$$

$$H = -s_{\theta'} R_1 + c_{\theta'} R_2 + (t_\beta s_\xi)\left(I_1 + \frac{(\tilde{m}_1)_{13}}{(\tilde{m}_0)_{33}} I_2 \right); \tag{A6}$$

$$m_\eta = \frac{v t_\beta s_\xi}{\sqrt{2}} \sqrt{(\tilde{m}_2)_{11} - \frac{(\tilde{m}_1)_{12}^2}{(\tilde{m}_0)_{22}} - \frac{(\tilde{m}_1)_{13}^2}{(\tilde{m}_0)_{33}}}. \tag{A7}$$

Here

$$\theta' = \theta + \frac{(t_\beta s_\xi)(\tilde{m}_1)_{23}}{(\tilde{m}_0)_{22} - (\tilde{m}_0)_{33}}. \tag{A8}$$

The scalar self-interactions,

$$\mathcal{L} = -\sum \left(\frac{1}{S_{ijk}} g_{ijk} v h_i h_j h_k + \frac{1}{S_{ijkl}} g_{ijk} h_i h_j h_k h_l \right), \tag{A9}$$

where the symmetric factor $S \equiv \prod(n_i!)$ and n_i denotes the appearance time for h_i in the Lagrangian. The couplings can be obtained directly from

$$g_{ijk} = \frac{1}{v} \frac{\partial^3 V}{\partial h_i \partial h_j \partial h_k}\bigg|_{\text{all } h_i = 0}, \quad g_{ijkl} = \frac{\partial^4 V}{\partial h_i \partial h_j \partial h_k \partial h_l}\bigg|_{\text{all } h_i = 0}. \tag{A10}$$

As an example, the $h\eta\eta$ vertex is given by

$$\begin{aligned} g_{h\eta\eta} &= \frac{\partial^3 V}{\partial h \partial \eta^2} \\ &= (\lambda_3 + \lambda_7) c_{\theta'} + \frac{1}{2} \lambda_5 s_{\theta'} - \frac{t_\beta c_\xi}{2} (\lambda_2 c_{\theta'} + (\lambda_4 - \lambda_7) s_{\theta'}). \end{aligned} \tag{A11}$$

For $m_\eta < m_h/2$, the strict constraints from the $h \to \eta\eta$ rare decay showed that

$$\lambda_3 + \lambda_7 + \frac{\lambda_5 t_{\theta'}}{2} \simeq \frac{t_\beta c_\xi}{2} (\lambda_2 + (\lambda_4 - \lambda_7) t_{\theta'}), \tag{A12}$$

which means we can ignore $(\tilde{m}_1)_{12} \sim \mathcal{O}(\beta)$ in the formula above.

For the $h_i VV$ and $h_i h_j Z$ couplings, the effective interaction should be written as

$$\mathcal{L}_{h_i VV} = c_{i,V} h_i \left(\frac{2 m_W^2}{v} W^{+\mu} W^-_\mu + \frac{m_Z^2}{v} Z^\mu Z_\mu \right); \tag{A13}$$

$$\mathcal{L}_{h_i h_j Z} = \frac{c_{ij} g}{2 c_W} Z^\mu (h_i \partial_\mu h_j - h_j \partial_\mu h_i). \tag{A14}$$

With a straightforward calculation, we have

$$c_{\eta,V} = c_{hH}, \qquad c_{h,V} = c_{H\eta}, \qquad c_{H,V} = c_{\eta h}; \tag{A15}$$

thus, $\sum c_{i,V}^2 = \sum c_{ij}^2 = 1$. In this scenario, to the leading order of $t_\beta s_\xi$,

$$c_{\eta,V} = t_\beta s_\xi \left(1 + s_\theta \frac{(\tilde{m}_1)_{13}}{(\tilde{m}_0)_{33}} - c_\theta \frac{(\tilde{m}_1)_{12}}{(\tilde{m}_0)_{22}} \right); \tag{A16}$$

$$c_{h,V} = c_{\theta'} + t_\beta c_\xi s_{\theta'}; \tag{A17}$$

$$c_{H,V} = -s_{\theta'} + t_\beta c_\xi c_{\theta'}. \tag{A18}$$

For the case $m_\eta < m_h - m_Z$, strict constraints from the $h \to Z\eta$ rare decay showed that $c_{H,V} \ll 1$; thus, $t_{\theta'} \simeq t_\beta c_\xi$.

The Yukawa interactions are

$$\begin{aligned} \mathcal{L}_Y = -\sum_\phi \Bigg(& \sum_f \frac{c_{\phi,f} m_f}{v} \bar{f}_L f_R \phi \\ & + \sum_{i \neq j} \frac{c_{\phi,ij} \sqrt{m_i m_j}}{v} \bar{f}_{Li} f_{Rj} \phi \Bigg) + \text{H.c.}, \end{aligned} \tag{A19}$$

where ϕ denotes any scalar and f denotes any fermion. The factors for diagonal terms can be generated directly as

$$\begin{aligned} c_{\eta,f} = & \pm i \xi_{ff} \left(1 + t_\beta s_\xi \left(\frac{(\tilde{m}_1)_{12}}{(\tilde{m}_0)_{22}} c_{\theta'} - \frac{(\tilde{m}_1)_{13}}{(\tilde{m}_0)_{33}} s_{\theta'} \right) \right) \\ & + t_\beta s_\xi \left(1 - c_{\theta'} \left(\xi_{ff} \frac{(\tilde{m}_1)_{12}}{(\tilde{m}_0)_{22}} + \frac{(\tilde{m}_1)_{13}}{(\tilde{m}_0)_{33}} \right) \right. \\ & \left. - s_{\theta'} \left(\xi_{ff} \frac{(\tilde{m}_1)_{12}}{(\tilde{m}_0)_{22}} - \frac{(\tilde{m}_1)_{13}}{(\tilde{m}_0)_{33}} \right) \right); \end{aligned} \tag{A20}$$

$$\begin{aligned} c_{h,f} = & c_{\theta'} + \xi_{ff} s_{\theta'} + t_\beta c_\xi (s_{\theta'} - \xi_{ff} c_{\theta'}) \\ & \pm i t_\beta s_\xi \xi_{ff} \left(\frac{(\tilde{m}_1)_{12}}{(\tilde{m}_0)_{22}} - c_{\theta'} \right); \end{aligned} \tag{A21}$$

$$\begin{aligned} c_{H,f} = & -s_{\theta'} + \xi_{ff} c_{\theta'} + t_\beta c_\xi (c_{\theta'} + \xi_{ff} s_{\theta'}) \\ & \pm i t_\beta s_\xi \xi_{ff} \left(\frac{(\tilde{m}_1)_{13}}{(\tilde{m}_0)_{33}} + s_{\theta'} \right), \end{aligned} \tag{A22}$$

while the factors for the off-diagonal term are

$$\begin{aligned} c_{\eta,ij} = & \pm i \xi_{ij} \left(1 + t_\beta s_\xi \left(\frac{(\tilde{m}_1)_{12}}{(\tilde{m}_0)_{22}} c_{\theta'} - \frac{(\tilde{m}_1)_{13}}{(\tilde{m}_0)_{33}} s_{\theta'} \right) \right) \\ & - t_\beta s_\xi \xi_{ij} \left(c_{\theta'} \frac{(\tilde{m}_1)_{13}}{(\tilde{m}_0)_{33}} + s_{\theta'} \frac{(\tilde{m}_1)_{12}}{(\tilde{m}_0)_{22}} \right); \end{aligned} \tag{A23}$$

$$c_{h,ij} = \xi_{ij} \left(s_{\theta'} - t_\beta c_\xi c_{\theta'} \pm i t_\beta s_\xi \left(\frac{(\tilde{m}_1)_{12}}{(\tilde{m}_0)_{22}} - c_{\theta'} \right) \right); \tag{A24}$$

$$c_{H,ij} = \xi_{ij}\left(c_{\theta'} + t_\beta c_\xi s_{\theta'} \pm i t_\beta s_\xi \left(\frac{(\tilde{m}_1)_{13}}{(\tilde{m}_0)_{33}} + s_{\theta'}\right)\right). \quad \text{(A25)}$$

In each of the six formulas, when "±" appears, "+" stands for down-type fermions and "−" stands for up-type fermions.

APPENDIX B: USEFUL ANALYTICAL LOOP INTEGRATIONS

The loop integration functions for the $h \to \gamma\gamma(gg)$ decay width in (40) and (41) are

$$\mathcal{A}_0(x) = \frac{x - f(x)}{x^2}, \quad \text{(B1)}$$

$$\mathcal{A}_{1/2}(x) = -\frac{x + (x-1)f(x)}{x^2}, \quad \text{(B2)}$$

$$\mathcal{B}_{1/2}(x) = -\frac{2f(x)}{x}, \quad \text{(B3)}$$

$$\mathcal{A}_1(x) = \frac{2x^2 + 3x + 3(2x-1)f(x)}{x^2}, \quad \text{(B4)}$$

where

$$f(x) = \begin{cases} \arcsin^2(\sqrt{x}), & (\text{for } x \le 1); \\ -\frac{1}{4}(\ln\frac{1+\sqrt{1-x^{-1}}}{1-\sqrt{1-x^{-1}}} - i\pi), & (\text{for } x > 1). \end{cases} \quad \text{(B5)}$$

The difference between $\mathcal{A}_{1/2}$ and $\mathcal{B}_{1/2}$ comes from the different tensor structures for the scalar and pseudoscalar components.

The loop integration functions for the oblique parameters in (50) and (51) are

$$F(x,y) = \frac{x+y}{2} - \frac{xy}{x-y}\ln\left(\frac{x}{y}\right); \quad \text{(B6)}$$

$$\begin{aligned} G(x,y) = &-\frac{16}{3} + 5(x+y) - 2(x-y)^2 \\ &+ 3\left(\frac{x^2+y^2}{x-y} + y^2 - x^2 + \frac{(x-y)^3}{3}\right)\ln\left(\frac{x}{y}\right) \\ &+ (1 - 2(x+y) + (x-y)^2) \\ &\times f(x+y-1, 1-2(x+y)+(x-y)^2); \end{aligned} \quad \text{(B7)}$$

$$\begin{aligned} H(x) = &-\frac{79}{3} + 9x - 2x^2 \\ &+ \left(-10 + 18x - 6x^2 + x^3 - 9\frac{x+1}{x-1}\right)\ln x \\ &+ (12 - 4x + x^2) f(x, x^2 - 4x), \end{aligned} \quad \text{(B8)}$$

where

$$f(x,y) = \begin{cases} \sqrt{y}\ln\left|\frac{x-\sqrt{y}}{x+\sqrt{y}}\right|, & y \ge 0; \\ 2\sqrt{-y}\arctan\left(\frac{\sqrt{-y}}{x}\right), & y < 0. \end{cases} \quad \text{(B9)}$$

The loop integration functions for meson mixing in (55) and (57) are

$$\mathcal{F}_0(x) = \frac{x(1 - x^2 + 2x\ln x)}{(1-x)^3}; \quad \text{(B10)}$$

$$\begin{aligned} \mathcal{F}_1(x,y,z) = &\frac{2y}{1-z}\left(\frac{(z-4)\ln y}{(1-y)^2} + \frac{3z\ln x}{(1-x)^2}\right. \\ &\left. - \frac{(1-z)(4-x)}{(1-y)(1-x)}\right); \end{aligned} \quad \text{(B11)}$$

$$\mathcal{F}_2(x) = 1 + \frac{9}{1-x} - \frac{6}{(1-x)^2} - \frac{6x^2\ln x}{(1-x)^3}. \quad \text{(B12)}$$

The loop integration functions for two-loop radiative LFV τ decay in (74) are

$$f(z) = \frac{z}{2}\int_0^1 dx \frac{1 - 2x(1-x)}{x(1-x) - z}\ln\left(\frac{x(1-x)}{z}\right); \quad \text{(B13)}$$

$$g(z) = \frac{z}{2}\int_0^1 dx \frac{1}{x(1-x) - z}\ln\left(\frac{x(1-x)}{z}\right); \quad \text{(B14)}$$

$$\begin{aligned} h(z) = &-\frac{z}{2}\int_0^1 dx \frac{1}{x(1-x) - z} \\ &\times \left(1 - \frac{z}{x(1-x)-z}\ln\left(\frac{x(1-x)}{z}\right)\right). \end{aligned} \quad \text{(B15)}$$

For $z < 1/4$, the integrations are defined as their Cauchy principle value.

The loop integration functions for the two-loop Barr-Zee-type contribution in calculating the EDM for a fermion f in (87) are

$$\mathcal{J}_0(m_\pm, m_\phi) = \frac{v^2}{2m_\phi^2}\left(\mathcal{I}\left(\frac{m_\pm^2}{m_\phi^2}\right) - \mathcal{I}'\left(\frac{m_\pm^2}{m_\phi^2}\right)\right); \quad \text{(B16)}$$

$$\mathcal{J}_{1/2}(m_t, m_\phi) = \frac{m_t^2}{m_\phi^2}\mathcal{I}\left(\frac{m_t^2}{m_\phi^2}\right); \quad \text{(B17)}$$

$$\mathcal{J}'_{1/2}(m_t, m_\phi) = \frac{m_t^2}{m_\phi^2}\mathcal{I}'\left(\frac{m_t^2}{m_\phi^2}\right); \quad \text{(B18)}$$

$$\begin{aligned} \mathcal{J}_1(m_W, m_\phi) = \frac{m_W^2}{m_\phi^2}\left(\left(5 - \frac{m_\phi^2}{2m_W^2}\right)\mathcal{I}\left(\frac{m_W^2}{m_\phi^2}\right)\right. \\ \left. + \left(3 + \frac{m_\phi^2}{2m_W^2}\right)\mathcal{I}'\left(\frac{m_W^2}{m_\phi^2}\right)\right), \end{aligned} \quad \text{(B19)}$$

where

$$\mathcal{I}(z) = \int_0^1 dx \frac{1}{x(1-x)-z} \ln\left(\frac{x(1-x)}{z}\right); \tag{B20}$$

$$\mathcal{I}'(z) = \int_0^1 dx \frac{1-2x(1-x)}{x(1-x)-z} \ln\left(\frac{x(1-x)}{z}\right). \tag{B21}$$

For $z < 1/4$, the integrations are defined as their Cauchy principle value as above. The loop function for the Weinberg operator in (91) is

$$\mathcal{K}(x) = 4x^2 \int_0^1 du \int_0^1 dv \frac{(uv)^3(1-v)}{(xv(1-uv)+(1-u)(1-v))^2}. \tag{B22}$$

The loop functions for the one-loop contribution to the fermion EDM in (93)–(94) and (98) are

$$\mathcal{P}_1(x) = \frac{x}{(x-1)^2}\left(\frac{x-3}{2} + \frac{\ln x}{x-1}\right); \tag{B23}$$

$$\mathcal{P}_2(x) = \int_0^1 dz \frac{z^2}{1-z+xz^2}. \tag{B24}$$

The loop integration functions for B-*meson* leptonic decays in (95) are

$$\mathcal{Y}_{\rm SM}(x) = \frac{x}{8}\left(\frac{x-4}{x-1} + \frac{3x\ln x}{(x-1)^2}\right); \tag{B25}$$

$$\mathcal{Y}_{\rm 2HDM}(x) = \frac{x^2}{8}\left(\frac{1}{y-x} + \frac{y}{(y-x)^2}\ln\left(\frac{x}{y}\right)\right). \tag{B26}$$

APPENDIX C: FORMALISM FOR MESON MIXING

We begin with the Schrödinger equation,

$$\mathrm{i}\frac{\partial}{\partial t}|\psi\rangle = \mathcal{H}|\psi\rangle = \left(\mathbf{m} - \frac{\mathrm{i}}{2}\mathbf{\Gamma}\right)|\psi\rangle, \tag{C1}$$

where $|\psi\rangle = (|M^0\rangle, |\bar{M}^0\rangle)^T$ with the normalization condition $\langle M^0|M^0\rangle = \langle\bar{M}^0|\bar{M}^0\rangle = 2m_M$ in position space, and $\mathbf{m}$, Γ are 2×2 matrixes. The Hamiltonian can be written as

$$\mathcal{H} = \mathcal{H}_0 + \mathcal{H}_{\Delta F=1} + \mathcal{H}_{\Delta F=2}. \tag{C2}$$

The matrix element is

$$\left(\mathbf{m} - \frac{\mathrm{i}}{2}\mathbf{\Gamma}\right)_{ij} = m_M\delta_{ij} + \frac{1}{2m_M}\langle\psi_i|\mathcal{H}_{\Delta F=2}|\psi_j\rangle + \frac{1}{2m_M} \times \int d\Pi_f \frac{\langle\psi_i|\mathcal{H}_{\Delta F=1}|f\rangle\langle f|\mathcal{H}_{\Delta F=1}|\psi_j\rangle}{m_M - E_f + \mathrm{i}\epsilon}, \tag{C3}$$

where the states $|\psi_{i,j}\rangle$ mean $|M^0\rangle$ or $|\bar{M}^0\rangle$, and $|f\rangle$ denotes a mediated state. The second and third terms correspond to short- and long-distance contributions, respectively, and from the third term,

$$\mathbf{\Gamma}_{ij} = \frac{1}{2m_M}\int d\Pi_f \langle\psi_i|\mathcal{H}_{\Delta F=1}|f\rangle\langle f|\mathcal{H}_{\Delta F=1}|\psi_j\rangle \times 2\pi\delta(E_f - m_M). \tag{C4}$$

The masses and widths for the mass eigenstates are

$$m_{H(L)} = m_M \pm \mathrm{Re}\left(\sqrt{\left(\mathbf{m}_{12} - \frac{\mathrm{i}}{2}\mathbf{\Gamma}_{12}\right)\left(\mathbf{m}_{12}^* - \frac{\mathrm{i}}{2}\mathbf{\Gamma}_{12}^*\right)}\right), \tag{C5}$$

$$\Gamma_{H(L)} = \Gamma_M \mp \mathrm{Im}\left(\sqrt{\left(\mathbf{m}_{12} - \frac{\mathrm{i}}{2}\mathbf{\Gamma}_{12}\right)\left(\mathbf{m}_{12}^* - \frac{\mathrm{i}}{2}\mathbf{\Gamma}_{12}^*\right)}\right), \tag{C6}$$

where H (L) denotes the heavy (light) mass eigenstate

$$|M_{H(L)}\rangle = p|M^0\rangle \mp q|\bar{M}^0\rangle. \tag{C7}$$

p and q are determined through

$$|p|^2 + |q|^2 = 1 \quad \text{and} \quad \left(\frac{p}{q}\right)^2 = \frac{\mathbf{m}_{12} - \mathrm{i}\mathbf{\Gamma}_{12}/2}{\mathbf{m}_{12}^* - \mathrm{i}\mathbf{\Gamma}_{12}^*/2}. \tag{C8}$$

In the $K^0 - \bar{K}^0$ system, $\mathbf{m}_{12}$ is almost real and $\Gamma_{12} \sim \mathbf{m}_{12}$; thus, $\Delta m_K \approx 2\mathrm{Re}\mathbf{m}_{12}$, while in the $B^0_{(s)} - \bar{B}^0_{(s)}$ system, $|\mathbf{\Gamma}_{12}| \ll |\mathbf{m}_{12}|$ and, thus, $\Delta m_B \approx 2|\mathbf{m}_{12}|$.

To transform to momentum space, we take $\mathcal{H}$ as the Hamiltonian density and change the normalization condition to $\langle M^0|M^0\rangle = \langle\bar{M}^0|\bar{M}^0\rangle = 2m_M\delta^{(3)}(\mathbf{p})$, with the matrix elements

$$\langle 0|\bar{f}_i\gamma^\mu\gamma^5 f_j|M^0(p)\rangle = -\mathrm{i}f_M p^\mu,$$
$$\langle 0|\bar{f}_i\gamma^5 f_j|M^0(p)\rangle = \mathrm{i}\frac{m_M^2 f_M}{m_i + m_j} \tag{C9}$$

and the useful $\Delta F = 2$ matrix elements

$$\begin{aligned}&\langle \bar{M}_0|\bar{f}_{Li}\gamma^\mu f_{Lj}\bar{f}_{Li}\gamma_\mu f_{Lj}|M_0\rangle \\ &= \langle \bar{M}_0|\bar{f}_{Ri}\gamma^\mu f_{Rj}\bar{f}_{Ri}\gamma_\mu f_{Rj}|M_0\rangle \\ &= \frac{2}{3}f_M^2 m_M^2; \end{aligned} \tag{C10}$$

$$\langle \bar{M}_0|\bar{f}_{Li}\gamma^\mu f_{Lj}\bar{f}_{Ri}\gamma_\mu f_{Rj}|M_0\rangle = -\frac{5}{6}f_M^2 m_M^2; \tag{C11}$$

$$\begin{aligned}\langle \bar{M}_0|\bar{f}_{Li}f_{Rj}\bar{f}_{Li}f_{Rj}|M_0\rangle &= \langle \bar{M}_0|\bar{f}_{Ri}f_{Lj}\bar{f}_{Ri}f_{Lj}|M_0\rangle \\ &= -\frac{5}{12}f_M^2 m_M^2; \end{aligned} \tag{C12}$$

$$\langle \bar{M}_0|\bar{f}_{Li}f_{Rj}\bar{f}_{Ri}f_{Lj}|M_0\rangle = \frac{7}{12}f_M^2 m_M^2, \tag{C13}$$

where the bag parameters are all taken as 1 for simplicity.

[1] Y.-N. Mao and S.-H. Zhu, Phys. Rev. D **90**, 115024 (2014).
[2] F. Englert and R. Brout, Phys. Rev. Lett. **13**, 321 (1964); P. W. Higgs, Phys. Rev. Lett. **13**, 508 (1964); G. S. Guralnik, C. R. Hagen, and T. W. B. Kibble, Phys. Rev. Lett. **13**, 585 (1964).
[3] G. C. Branco, P. M. Ferreira, L. Lavoura, M. N. Rebelo, M. Sher, and J. P. Silva, Phys. Rep. **516**, 1 (2012).
[4] G. Aad *et al.* (The ATLAS Collaboration), Phys. Lett. B **716**, 1 (2012).
[5] S. Chatrchyan *et al.* (The CMS Collaboration), Phys. Lett. B **716**, 30 (2012).
[6] G. Aad *et al.* (The ATLAS and CMS Collaborations), Phys. Rev. Lett. **114**, 191803 (2015).
[7] The ATLAS Collaboration, CERN Report No. ATLAS-CONF-2015-007 2015.
[8] M. Flechl (The ATLAS and CMS Collaborations), J. Phys. Conf. Ser. **631**, 012028 (2015).
[9] The ATLAS and CMS Collaborations, CERN Report No. ATLAS-CONF-2015-044 2015.
[10] J. Ellis, J. F. Gunion, H. E. Haber, L. Roszkowski, and F. Zwirner, Phys. Rev. D **39**, 844 (1989).
[11] D. E. Kaplan and M. Schmaltz, J. High Energy Phys. 10 (2003) 039.
[12] K. Cheung and J. Song, Phys. Rev. D **76**, 035007 (2007).
[13] K. Cheung, J. Song, P. Tseng, and Q.-S. Yan, Phys. Rev. D **78**, 055015 (2008).
[14] Z. Chacko, H.-S. Goh, and R. Harnik, Phys. Rev. Lett. **96**, 231802 (2006); J. High Energy Phys. 01 (2006) 108.
[15] Y.-B. Liu and Z.-J. Xiao, J. High Energy Phys. 02 (2014) 128.
[16] J.-M. Gérard and M. Herquet, Phys. Rev. Lett. **98**, 251802 (2007).
[17] B. Coleppa, F. Kling, and S. Su, J. High Energy Phys. 01 (2014) 161.
[18] L. Wang and X.-F. Han, J. High Energy Phys. 05 (2015) 039.
[19] B. Dumont, J. F. Gunion, Y. Jiang, and S. Kraml, Phys. Rev. D **90**, 035021 (2014).
[20] J. Bernon, J. F. Gunion, Y. Jiang, and S. Kraml, Phys. Rev. D **91**, 075019 (2015).
[21] D. Curtin *et al.*, Phys. Rev. D **90**, 075004 (2014).
[22] S. Chatrchyan *et al.* (The CMS Collaboration), Phys. Rev. D **89**, 092007 (2014).
[23] The CMS Collaboration, CERN Report No. CMS-PAS-HIG-14-014 2014.
[24] The ATLAS Collaboration, CERN Report No. ATLAS-CONF-2015-008 2015.
[25] M. Kobayashi and T. Maskawa, Prog. Theor. Phys. **49**, 652 (1973).
[26] N. Cabbibo, Phys. Rev. Lett. **10**, 531 (1963).
[27] L. Wolfenstein, Phys. Rev. Lett. **51**, 1945 (1983).
[28] C. Jarlskog, Phys. Rev. Lett. **55**, 1039 (1985).
[29] K. A. Olive *et al.* (Particle Data Group), Chin. Phys. C **38**, 090001 (2014).
[30] P. A. R. Ade *et al.* (The Planck Collaboration), Astron. Astrophys. **571**, A16 (2014).
[31] A. G. Cohen, D. B. Kaplan, and A. E. Nelson, Phys. Lett. B **263**, 86 (1991); Annu. Rev. Nucl. Part. Sci. **43**, 27 (1993).
[32] D. E. Morrissey and M. J. Ramsey-Musolf, New J. Phys. **14**, 125003 (2012).
[33] J. Shu and Y. Zhang, Phys. Rev. Lett. **111**, 091801 (2013).
[34] T. D. Lee, Phys. Rev. D **8**, 1226 (1973); Phys. Rep. **9**, 143 (1974).
[35] A. Méndez and A. Pomaral, Phys. Lett. B **272**, 313 (1991).
[36] S.-H. Zhu, arXiv:1410.2042.
[37] J. D. Bjorken and S. Weinberg, Phys. Rev. Lett. **38**, 622 (1977).
[38] S. L. Chen, N. G. Deshpande, X. G. He, J. Jiang, and L. H. Tsai, Eur. Phys. J. C **53**, 607 (2008).
[39] W. Liao, http://125.217.162.12/~zhanghonghao/tev2014/tev2014ppt/TeV2014_3a_Liaowei.pdf.
[40] T. P. Cheng and M. Sher, Phys. Rev. D **35**, 3484 (1987).
[41] B. Pontecorvo, Zh. Eksp. Teor. Fiz. **33**, 549 (1957) [Sov. Phys. JEPT **6**, 429 (1957)]; Z. Maki, M. Nakagawa, and S. Sakata, Prog. Theor. Phys. **28**, 870 (1962).
[42] M. Ablikim *et al.* (BESIII Collaboration), Reports No. BAM-00180 and No. BAM-000402; Phys. Rev. D **93**, 052005 (2016).
[43] B. Aubert *et al.* (*BABAR* Collaboration), Phys. Rev. Lett. **103**, 081803 (2009).
[44] V. Prasad, SLAC Reports No. SLAC-R-1008 and No. BABAR-THESIS-13-001 (Ph.D. Thesis).
[45] S. Chatrchyan *et al.* (The CMS Collaboration), Phys. Rev. Lett. **109**, 121801 (2012).
[46] The CMS Collaboration, CERN Report No. CMS-HIG-14-033 2016;Phys. Lett. B **758**, 296 (2016).

[47] The ACME Collaboration, Science **343**, 269 (2014).
[48] C. Baker *et al.*, Phys. Rev. Lett. **97**, 131801 (2006).
[49] M. Pospelov and A. Ritz, Ann. Phys. (Amsterdam) **318**, 119 (2005).
[50] G. Abbiendi *et al.* (ALEPH, DELPHI, L3, and OPAL Collaborations and the LEP Higgs Working Group), Phys. Lett. B **565**, 61 (2003).
[51] S. Schael *et al.* (The ALEPH, DELPHI, L3, OPAL Collaborations and LEP Higgs Working Group), Eur. Phys. J. C **47**, 547 (2006).
[52] The ALEPH, DELPHI, L3, OPAL Collaborations and LEP Higgs Working Group, Report No. LHWG Note/2001-04, arXiv:hep-ex/0107030.
[53] P. Mario (The CMS Collaboration), Report No. CMS-CR-2015-045.
[54] G. Aad *et al.* (The ATLAS Collaboration), J. High Energy Phys. 01 (2016) 032.
[55] The LHC Higgs Cross Section Working Group, Report No. CERN-2013-004.
[56] V. Khachatryan *et al.* (The CMS Collaboration), Phys. Lett. B **749**, 560 (2015).
[57] G. Aad *et al.* (The ATLAS Collaboration), Report No. CERN-PH-EP-2015-290; J. High Energy Phys. 03 (2016) 127.
[58] A. Djouadi, Phys. Rep. **457**, 1 (2008).
[59] A. Djouadi, Phys. Rep. **459**, 1 (2008).
[60] M. Baak, J. Cuth, J. Haller, A. Hoecker, R. Kogler, K. Mönig, M. Schott, and J. Stelzer, Eur. Phys. J. C **74**, 3046 (2014).
[61] M. E. Peskin and T. Takeuchi, Phys. Rev. Lett. **65**, 964 (1990); Phys. Rev. D **46**, 381 (1992).
[62] W. Grimus, L. Lavoura, O. M. Ogreid, and P. Osland, J. Phys. G **35**, 075001 (2008); Nucl. Phys. **B801**, 81 (2008).
[63] H. E. Haber and D. O'Neil, Phys. Rev. D **83**, 055017 (2011).
[64] R. M. Winters and D. O'Neil, http://people.bridgewater.edu/~doneil/STellipseModule.nb.
[65] The ALEPH, DELPHI, L3, OPAL Collaborations and LEP Higgs Working Group, Report No. LHWG Note/2001-05, arXiv:hep-ex/0107031.
[66] E. Cerveró and J.-M. Gérard, Phys. Lett. B **712**, 255 (2012).
[67] The Heavy Flavor Averaging Group, arXiv:1412.7515; see also http://www.slac.stanford.edu/xorg/hfag/.
[68] J. Yu, *Proc. Sci.*, LATTICE (2013) 398.
[69] A. Lenz, Reports No. IPPP/14/85 and No. DCPT/14/170.
[70] A. Lenz and U. Nierste, Reports No. TTP11-03 and No. TUM-HEP-792/11.
[71] A. Lenz, U. Nierste, J. Charles, S. Descotes-Genon, A. Jantsch, C. Kaufhold, H. Lacker, S. Monteil, V. Niess, and S. T'Jampens, Phys. Rev. D **83**, 036004 (2011).
[72] S. Aoki *et al.* (FLAG Working Group), Eur. Phys. J. C **74**, 2890 (2014).
[73] A. Hocker and Z. Ligeti, Annu. Rev. Nucl. Part. Sci. **56**, 501 (2006).
[74] J. Charles, S. Descotes-Genon, Z. Ligeti, S. Monteil, M. Papucci, and K. Trabelsi, Phys. Rev. D **89**, 033016 (2014).
[75] B. McWilliams and O. Shanker, Phys. Rev. D **22**, 2853 (1980).
[76] R. S. Gupta and J. D. Wells, Phys. Rev. D **81**, 055012 (2010).
[77] A. Lenz, U. Nierste, J. Charles, S. Descotes-Genon, H. Lacker, S. Monteil, V. Niess, and S. T'Jampens, Phys. Rev. D **86**, 033008 (2012).
[78] E. Golowich, J. A. Hewett, S. Pakvasa, and A. A. Petrov, Phys. Rev. D **76**, 095009 (2007).
[79] C. Q. Geng and J. N. Ng, Phys. Rev. D **38**, 2857 (1988).
[80] The ATLAS Collaboration, CERN Report No. CERN-PH-EP-2015-229 2015.
[81] K. G. Chetyrkin, R. Harlander, T. Seidensticker, and M. Steinhauser, Phys. Rev. D **60**, 114015 (1999).
[82] S. Chatrchyan *et al.* (The CMS Collaboration), J. High Energy Phys. 02 (2014) 024.
[83] M. Czakon, P. Fiedler, and A. Mitov, Phys. Rev. Lett. **110**, 252004 (2013).
[84] The CMS Collaboration, CERN Report No. CMS-PAS-SUS-13-013 2013.
[85] A. D. Martin, W. J. Stirling, R. S. Thorne, and G. Watt, Eur. Phys. J. C **63**, 189 (2009); see also http://mstwpdf.hepforge.org/.
[86] The CMS Collaboration, CERN Reports No. CMS-HIG-14-005 and No. CERN-PH-EP-2015-027 2015.
[87] The ATLAS Collaboration, CERN Report No. CERN-PH-EP-2015-184 2015.
[88] K. Hayasaka *et al.* (Belle Collaboration), Phys. Lett. B **666**, 16 (2008).
[89] B. Aubert *et al.* (*BABAR* Collaboration), Phys. Rev. Lett. **104**, 021802 (2010).
[90] J. Adam *et al.* (MEG Collaboration), Phys. Rev. Lett. **110**, 201801 (2013).
[91] W. J. Marciano and A. I. Sanda, Phys. Lett. **67B**, 303 (1977).
[92] Y.-N. Mao and S.-H. Zhu, Phys. Rev. D **93**, 035014 (2016).
[93] S. Davidson and G. Grenier, Phys. Rev. D **81**, 095016 (2010).
[94] Y. Omura, E. Senaha, and K. Tobe, J. High Energy Phys. 05 (2015) 028.
[95] Y. Omura, E. Senaha, and K. Tobe, arXiv:1511.08880.
[96] S. M. Barr and A. Zee, Phys. Rev. Lett. **65**, 21 (1990); **65**, 2920 (1990).
[97] D. Chang, W.-S. Hou, and W.-Y. Keung, Phys. Rev. D **48**, 217 (1993).
[98] R. Harnik, J. Kopp, and J. Zupan, J. High Energy Phys. 03 (2013) 026.
[99] G. 't Hooft, Phys. Rev. Lett. **37**, 8 (1976); J. E. Kim and G. Garosi, Rev. Mod. Phys. **82**, 557 (2010).
[100] J. Brod, U. Haisch, and J. Zupan, J. High Energy Phys. 11 (2013) 180.
[101] T. Abe, J. Hisano, T. Kitahara, and K. Tobioka, J. High Energy Phys. 01 (2014) 106.
[102] K. Cheung, J. S. Lee, E. Senaha, and P.-Y. Tseng, J. High Energy Phys. 06 (2014) 149.
[103] L. Bian, T. Liu, and J. Shu, Phys. Rev. Lett. **115**, 021801 (2015).
[104] A. Soni and R. M. Xu, Phys. Rev. Lett. **69**, 33 (1992).
[105] D. Atwood, S. Bar-Shalom, G. Eilam, and A. Soni, Phys. Rep. **347**, 1 (2001).
[106] S. Weinberg, Phys. Rev. Lett. **63**, 2333 (1989); D. A. Dicus, Phys. Rev. D **41**, 999 (1990).

[107] E. Braaten, C.-S. Li, and T.-C. Yuan, Phys. Rev. Lett. **64**, 1709 (1990).
[108] S. Chatrchyan *et al.* (The CMS Collaboration), Eur. Phys. J. C **73**, 2604 (2013).
[109] S. Chatrchyan *et al.* (The CMS Collaboration), Phys. Rev. Lett. **111**, 101804 (2013).
[110] R. Aaij *et al.* (The LHCb Collaboration), Phys. Rev. Lett. **111**, 101805 (2013).
[111] V. Khachatryan *et al.* (The CMS and LHCb Collaborations), Nature (London) **522**, 68 (2015).
[112] A. J. Buras, J. Girrbach, D. Guadagnoli, and G. Isidori, Eur. Phys. J. C **72**, 2172 (2012).
[113] C. Bobeth, M. Gorbahn, T. Hermann, M. Misiak, E. Stamou, and M. Steinhauser, Phys. Rev. Lett. **112**, 101801 (2014); T. Hermann, M. Misiak, and M. Steinhauser, J. High Energy Phys. 12 (2013) 097.
[114] X.-Q. Li, J. Lu, and A. Pich, J. High Energy Phys. 06 (2014) 022.
[115] M. Misiak *et al.*, Phys. Rev. Lett. **114**, 221801 (2015); M. Czakon, P. Fiedler, T. Huber, M. Misiak, T. Schutzmeier, and M. Steinhauser, J. High Energy Phys. 04 (2015) 168.
[116] T. Hermann, M. Misiak, and M. Steinhauser, J. High Energy Phys. 11 (2012) 036; see also the MATHEMATICA code at http://www.ttp.kit.edu/Progdata/ttp12/ttp12-29/.
[117] M. Casolino, T. Farooque, A. Juste, T. Liu, and M. Spannowsky, Eur. Phys. J. C **75**, 498 (2015).
[118] J. L. Abelleira Fernandez *et al.* (LHeC Study Group), J. Phys. G **39**, 075001 (2012).
[119] E. Cruz-Alaniz, D. Newton, R. Tomás, and M. Korostelev, Phys. Rev. ST Accel. Beams **18**, 111001 (2015).
[120] Y.-L. Tang, C. Zhang, and S.-H. Zhu, Phys. Rev. D **94**, 011702 (2016).
[121] M. Bicer *et al.* (TLEP Design Study Working Group), J. High Energy Phys. 01 (2014) 164.
[122] M. Aicheler *et al.*, Reports No. CERN-2012-007, No. SLAC-R-985, No. KEK-Report-2012-1, No. PSI-12-01, and No. JAI-2012-001 2012.
[123] M. Ahmad *et al.* (CEPC-SPPC Study Group), Reports No. IHEP-CEPC-DR-2015-01, No. IHEP-TH-2015-01, and No. IHEP-EP-2015-01, http://cepc.ihep.ac.cn/preCDR/volume.html 2015.
[124] C. Adolphsen *et al.*, arXiv:1306.6328; arXiv:1306.6353.
[125] CMS Collaboration, CERNReport No. CMS-PAS-FTR-13-024 2013.
[126] LHC Higgs Cross Section Working Group, CERN Report No. CERN-2011-002 2011.
[127] C. S. Huang and S.-H. Zhu, Phys. Rev. D **60**, 075012 (1999); S.-H. Zhu, Phys. Rev. D **67**, 075006 (2003).
[128] K. Huitu, S. K. Rai, K. Rao, S. D. Rindani, and P. Sharma, J. High Energy Phys. 04 (2011) 026.
[129] X. Gong, Z.-G. Si, S. Yang, and Y.-J. Zheng, Phys. Rev. D **87**, 035014 (2013).
[130] Q.-H. Cao, X. Wan, X.-P. Wang, and S.-H. Zhu, Phys. Rev. D **87**, 055022 (2013).
[131] D. Asner *et al.*, arXiv:1310.0763.
[132] M. Battaglia, A. Ferrari, A. Kiiskinen, and T. Maki, eConf C010630, E3017 (2001).
[133] Y.-N. Mao, Ph. D. Thesis (2016); G. Li, Y.-N. Mao, C. Zhang, and S.-H. Zhu (to be published); G. Li, Y.-N. Mao, and S.-H. Zhu (to be published).
[134] The CMS Collaboration, Report No. CMS-NOTE-13-002.
[135] The ATLAS Collaboration, CERN Report No. ATL-PHYS-PUB-2013-007; Report No. ATL-PHYS-PUB-2013-014 2013.
[136] S. Berge, W. Bernreuther, and J. Ziethe, Phys. Rev. Lett. **100**, 171605 (2008); S. Berge, W. Bernreuther, and S. Kirchner, Phys. Rev. D **92**, 096012 (2015).
[137] S. Berge, W. Bernreuther, and H. Spiesberger, Phys. Lett. B **727**, 488 (2013).
[138] P. S. Bhupal Dev, A. Djouadi, R. M. Godbole, M. M. Mühlleitner, and S. D. Rindani, Phys. Rev. Lett. **100**, 051801 (2008); R. M. Godbole, C. Hangst, M. Mühlleitner, S. D. Rindani, and P. Sharma, Eur. Phys. J. C **71**, 1681 (2011).
[139] T. Aushev *et al.*, Report No. KEK Report 2009-12.
[140] SuperB Collaboration, Reports No. INFN/AE-10/2, No. LAL-110, and No. SLAC-R-952.
[141] S. Khatibi and M. M. Najafabadi, Phys. Rev. D **90**, 074014 (2014).
[142] LHCb Collaboration, CERN Reports No. CERN-LHCC-2011-001 and No. LHCC-I-018 2011; CERN Reports No. CERN-LHCC-2012-007 and No. LHCb-TDR-12 2012.
[143] The CMS Collaboration, CERN Report No. CMS-PAS-FTR-13-022 2013.
[144] J. Kopp and M. Nardecchia, J. High Energy Phys. 10 (2014) 156.
[145] E. Levichev, Phys. Part. Nucl. Lett. **5**, 554 (2008).
[146] A. V. Bobrov and A. E. Bondar, Nucl. Phys. B, Proc. Suppl. **225–227**, 195 (2012); **253–255**, 199 (2014).
[147] A. M. Baldini *et al.* (MEG Collaboration), arXiv:1301.7225.